Surface Property Modification of Copper By Nanocomposite Coating

A THESIS SUBMITTED IN PARTIAL FULFILMENT OF THE

REQUIREMENTS FOR THE DEGREE OF

Master of Technology
In
Metallurgical and Materials Engineering

Submitted by

Ashok Akarapu

Roll No. 209MM1232

Department of Metallurgical & Materials Engineering
National Institute of Technology
Rourkela
2010-2011

Surface Property Modification of Copper By Nanocomposite Coating

A THESIS SUBMITTED IN PARTIAL FULFILMENT OF THE

REQUIREMENTS FOR THE DEGREE OF

Master of Technology
In
Metallurgical and Materials Engineering

Submitted by

Ashok Akarapu

Roll No. 209MM1232

Under the supervision of

Prof. A. Basu and Prof. S.K. Pratihar

Department of Metallurgical & Materials Engineering
National Institute of Technology
Rourkela
2010-2011

National Institute Of Technology
Rourkela

<u>CERTIFICATE</u>

This is to certify that the thesis entitled, "**Surface Property Modification of Copper by Nanocomposite Coating**", submitted by **Ashok Akarapu** in partial fulfillment of the requirements for the award of Master of Technology Degree in **Metallurgical and Materials Engineering Department** at the National Institute of Technology, Rourkela is an authentic work carried out by him under our supervision and guidance.

To the best of our knowledge, the matter embodied in the thesis has not been submitted to any other University/ Institute for the award of any degree or diploma.

Prof. A. Basu
Dept. Metallurgical & Materials Engineering
National Institute of Technology
Rourkela-769008.
Date:

Prof. S.K. Pratihar
Dept. Ceramic Engineering
National Institute of Technology
Rourkela-769008.
Date:

ACKNOWLEDGEMENT

LIST OF FIGURES

LIST OF TABLES

Abstract

Copper has high electrical and thermal conductivities, good corrosion resistance at ambient temperature, excellent malleability/workability and reproducibility, apart from these it is cheap and abundantly available metal other than good conducting metals like Silver. But has poor mechanical properties such as hardness and wear resistance. Some applications like Contacts in electrical switches necessitate the improvements in the mechanical properties without much loss of electrical and thermal conductivities. Bulk modification / alloying have been tried but limitations in alloying and adversely decrease in its electrical and thermal conductivities has been reported. Another way to improve its mechanical properties is with Surface modification by developing composite coating on its surface. In the present work we employed Electrodeposition process to develop a composite coating with Cu matrix and Ceramic oxide particles TiO_2 (particle size ~202 nm), Al_2O_3 (particle size ~287 nm) as reinforcements. The coatings were developed with 10 g/l, 30 g/l and 0 g/l (unreinforced) concentrations in bath, at four different current densities (5, 8, 11, 14 A/dm^2) with using copper sulfate bath in order to study the effect of Current density and particle concentration in bath, on structure and properties of the coatings developed. The crystallite size was averagely 50-65 nm and a strong (220) texture was obtained in composite coatings and unreinforced Cu coatings determined from the XRD data. The composition and surface morphology of coatings were studied by using EDS and SEM. Hardness and Wear resistance of the coatings were determined by using microhardness tester and ball on plate wear tester, improved hardness and wear resistance of composite coatings were observed compared to the unreinforced copper coatings.

Keywords: Electrodeposition, Electrocodeposition, TiO_2, Al_2O_3, copper, texture, microhardness, wear.

CONTENTS

Chapter 1

Introduction

Introduction

Objectives and Scope of the Present study

Scope of the thesis

CHAPTER 1

INTRODUCTION

1.1 Introduction

Copper (Cu) is environment friendly and abundantly available material that possesses a unique combination of low electrical resistivity (16.78×10^{-9} Ωm) and high thermal conductivity (394 $Wm^{-1}K^{-1}$), excellent malleability/workability, attractive colour, reasonably good corrosion resistance at ambient temperature [1] and recyclability, apart from these it is cheaper than the other conducting metals. Due to these excellent combination of properties Cu and its alloys are most widely used engineering materials for conduction of electricity (electrical conductors, wires, contacts, plugs) and heat (heat exchangers, linings, radiators, electrodes). However, poor mechanical property often necessitates strengthening without adversely affecting its electrical/thermal conductivity. Some applications like electrical contacts require mainly good surface mechanical properties like hardness, wear resistance due to frequent rubbing action during switching. Bulk modification/alloying decreases thermal and electrical conductivity and along with electrical conductivity, thermal conductivity is also important so that the contacts can quickly release the heat accumulated due to resistance heating and rubbing action during switching. In such components Surface Engineering approach is wise one as it does not adversely affect bulk properties like electrical and thermal conductivities compared to bulk modification. The wide variety of surface coating techniques available are Physical vapor deposition, Chemical vapor deposition, Thermal spraying, Electrodeposition, Electroless deposition, Diffusion coatings, and Laser based techniques (Laser Cladding, etc.).

Metal matrix nanocomposites containing dispersed second-phase particulates have various special properties such as dispersion hardening, self-lubricity, high temperature inertness, good wear and corrosion resistance, and chemical and biological compatibility [2–7]. Electrocodeposition has several advantages in developing Metal matrix composite coatings among other coating processes such as, uniform depositions on complexly shaped substrates, low cost, good reproducibility and the reduction of waste [8]. Electrocodeposition process has been in use successfully to develop such nanocomposite coatings from the past decades. The second phase can be hard oxide (Al_2O_3, TiO_2, SiO_2) [7] or carbides particles (SiC, WC) [7], etc.,

embedded in metals like Cu, Ni, Cr, Co and various alloys. The applications of these coatings include wear and abrasion resistant surfaces, lubrication, high hardness tools, dispersion-strengthened alloys, and for protection against oxidation and hot corrosion [7, 9 -11].

The quality of the deposits influenced by wide number of variables which include current density, particle characteristics, bath composition, hydrodynamics and the particle-bath interaction. The amount of embedded second phase particles plays an important role in improving the surface mechanical properties by refining the grain size of the matrix and also by dispersion strengthening mechanism. Several parameters affect the embedded vol.% of second phase particles, among which current density, particle concentration in the bath, and *pH* of the solution are important variables. Current density plays an important role in controlling the deposition rate which will in turn affect the concentration of incorporated particles in the coatings.

In the present work parallel plate electrodeposition process employed to improve the surface mechanical properties of copper without adversely effecting it's electrical and thermal conductivities, by developing a layer of nanocomposite coating consisting of copper matrix and ultrafine ceramic oxide particles (TiO_2, Al_2O_3) on surface of copper. And to determine the optimized current density and particle concentration in the bath with the coating results achieved.

1.2 Objectives and Scope of the Present study

The aim of the present work is to improve the surface mechanical properties of Cu by electro codeposition of Cu with dispersed second phase ultra fine particles like TiO_2, Al_2O_3 individually the objectives of the work as summarized below:

1. To determine the particle size and Zeta potential (for isoelectric point) of the ceramic oxide powders (TiO_2, Al_2O_3) procured from Inframat Advanced Materials, Formington, USA by using Malvern Zetasizer nano series Nano- ZS model instrument.

2. Electro codeposition of Cu with dispersed second phase ultra fine particles TiO_2, Al_2O_3 individually such that to develop Cu-TiO_2 and Cu-Al_2O_3 nanocomposite coatings uniformly on the surface of the Copper substrate.

3. Characterizations of The coatings developed

- Phase identification, texture analysis and Chemical analysis (XRD, EDS).
- Microstructure and Morphology (SEM, FESEM).
- Surface mechanical properties (Hardness, Wear).

4. Optimization of the process.

5. Correlation with process parameters.

1.3 Scope of the Thesis

The organization of the rest of the thesis is as follows: Different strengthening mechanisms of Cu, brief explanation about electrodeposition process with advantages over other coating techniques, applications and about electro codeposition, effect of different parameters on the properties of electro codeposited coatings, their applications and brief literature reviews on Cu-TiO_2 and Cu- Al_2O_3 composite coatings were provided in chapter 2. A detailed experimental study and about different characterizations techniques were provided in chapter 3. In chapter 4 a discussion about the results obtained from the characterizations of the powders (TiO_2, Al_2O_3) along with the mechanical property study of different co deposited samples were provided. In chapter 5 a summary of main findings and conclusions of the present work were reported. References were provided in chapter 6.

Chapter2

Literature Review

Strengthening Mechanisms of Copper

Surface Engineering

Electrodeposition

Pulsed Electrodeposition

Electrophoreticdeposition

Electrocodeposition

Brief Literature Reviews on Cu Nanocomposites

Wear and Various Wear Mechanisms

CHAPTER 2
LITERATURE REVIEW

2.1 Strengthening Mechanisms of Copper

2.1.1 Bulk modification

Copper have poor mechanical properties, usually the strength of the copper can be enhanced based on solid solution (substitutional/interstitial), precipitation (coherent/semi-coherent) and/or dispersion (externally added phases) strengthening mechanisms [12].

(a) Solid solution Strengthening / Alloying

Solid solution strengthening / alloying is the common process to improve the hardness and to strengthen the pure copper. When Small amounts of an alloying element added to molten copper will completely dissolve and form a homogeneous microstructure (a single phase). The common alloying elements used for copper are Zn, Sn, Be, Cr, Ag, Au, Ni, Al, As, Fe, etc., When tin added to copper the alloy formed is known as bronze the resulting alloy is stronger and harder than either of the pure metals. When Zn added to pure copper the alloy is known as Brass. Tin is more effective in strengthening copper than zinc, but is also more expensive and has a greater detrimental effect on the electrical and thermal conductivities than zinc. Aluminum (forming alloys known as aluminum bronzes), Manganese, Nickel, and Silicon can also be added to strengthen the copper.

(b) Precipitation hardening / Dispersion Strengthening

Precipitation hardening/ Dispersion Strengthening is another strengthening mechanism of copper. Both of the processes involves hindering or pinning of the dislocation motion in matrix phase and strengthens the matrix phase. Precipitation process involves quenching a supersaturated solid solution from an elevated temperature, then reheating to a lower temperature (aging) to allow the excess solute to precipitate out and form a second phase. This process is often used for copper alloys containing beryllium, chromium, nickel, or zirconium.

4

In Dispersion strengthening mechanism the strength of copper can be increased by finely dispersing small, hard and inert particles in copper matrix. The dispersed second phase particles again act as obstacles for dislocation motion same as in Precipitation hardening. They are not as effective in increasing the strength of materials compared to precipitates since their size is commonly larger than 10 nm and they are generally incoherent with the matrix. The main advantage, however, is that these foreign particles generally neither dissolve at high temperatures nor grow in size, as is known for precipitates. Thus, dispersion hardened materials maintain their strength even at high temperatures.

(c) Grain size Strengthening

The strength of the materials can also be increased by increasing the grain boundary surface area or decreasing the existing grain sizes to nanometers. The mechanism involved in increasing strength is that the small grain sizes acts as obstacles to the dislocation motion and thus increase in strength. According to the Hall-Petch relation the strength is inversely proportional to the square of the average grain diameter. (i.e., $\sigma_y = \sigma_0 + k\ d^{-1/2}$) where σ_y is the yield stress, σ_0 is friction stress, k is the locking parameter, and d is grain diameter.

However, bulk modification approach is widely investigated for improvement of mechanical properties of Cu and thereby improving the life of the Cu contacts. But bulk modification has restrictions on solubility limit, also adversely affecting the electrical and thermal conductivities. For example bulk alloying with Zn, Si, Sn and Al, though is effective in improving mechanical strength by solid solution strengthening but proves counterproductive by decreasing the mean free path of electrons and thereby increasing electrical resistivity [13]. On the other hand, Cr and Be are the only alloying elements that enhances mechanical strength of Cu without adversely affecting its electrical/thermal conductivity [14]. However, both Cr and Be have restricted solid solubility in Cu (e.g. 0.89 at. % Cr in Cu at 1000 °C) and Be is toxic, breathing of Cu-Be dust, as formed when machining or welding may cause serious lung damage [15].

Another way to improve the mechanical properties of Cu and hence copper contacts is by modifying the surface of the Cu contacts with hard coatings by using Surface Engineering Techniques without adversely affecting the bulk properties such as electrical and thermal conductivities of the contacts which are necessary for the contact applications.

2.2 Surface Engineering

Surface engineering is defined as branch of science that deals with the different techniques to achieve desired surface properties and their behavior in service for engineering components. Surface engineering techniques are being used in the automotive, aerospace, missile, power, electronic, biomedical, textile, petroleum, petrochemical, chemical, steel, power, cement, machine tools, and construction industries [16]. Surface engineering techniques can be used to develop a wide range of functional properties, including physical, chemical, electrical, electronic, magnetic, mechanical, wear-resistant and corrosion-resistant properties at the required substrate surfaces. Almost all types of materials, including metals, ceramics, polymers, and composites can be coated on similar or dissimilar materials.

Surface treatments that cause microstructure changes in the bulk material include heating and cooling/quenching through induction, flame, laser, and electron beam techniques, or mechanical treatments (one example is cold working). Surface treatments that alter the chemistry of a surface include carburizing, nitriding, nitrocarburizing, carbonitriding, boronizing, siliconizing, chromizing and aluminizing. Hard facing is another form of surface treatment, where the bulk material's surface is given a protective layer of another material having more superior properties than those of the bulk material. Each method of hard facing, examples of which are coating deposition, cladding or welding, causes particular physical and chemical effects on the bulk material, some beneficial, some detrimental [17]. The wide variety of Surface coating techniques available are Thermochemical coatings (carburizing, nitriding etc.), Spray Coatings (thermal spray coatings, Flame spray, Plasma spray coatings etc.), Electrodeposition, Electrolessdeposition, Physical Vapor deposition (Sputtering, Ion Plating, Ion Implantation etc.), Chemical Vapor deposition (Plasma Enhanced chemical vapor deposition etc.) and Laser Cladding, etc.,

2.2.1 Various Coating Techniques

(a) Electroplating

Electroplating is often also called "electrodeposition", a short version of electrolytic deposition, It's a process using electrical current to reduce cations of a desired material from a solution and coat that material as a thin film onto a conductive substrate surface.

(b) Electroless plating

Electroless plating processes involves no external current to reduce the metal cations into metal atoms. Metal coatings in this process are produced by chemical reduction with electrons supplied by a reducing agent (R.A.) present in the solution. The process was reported by Brenner and Riddell [18] in 1946 for nickel and cobalt coatings and has been using extension to electroless plating of copper, gold, palladium, platinum, silver and a variety of alloys involving one or more of these metals.

(c) Physical Vapor Deposition

Physical vapor deposition (PVD) includes a broad class of vacuum coating processes in which the material is physically removed from a source by evaporation or sputtering, transported through a vacuum and condensed as a film on the surfaces of appropriately placed parts or substrates. The thickness of the deposits can vary from angstroms to millimeters. PVD coatings are generally used to improve hardness, wear resistance and oxidation resistance. Thus such coatings use in wide range of applications such as Aerospace, Automotive, Medical / Surgical, Cutting Tools, etc., As this process is carried out in a vacuum chamber, the size limitation of the work piece is the drawback of this process. In addition the process is effectively line of sight so deep holes, bores and undercuts cannot easily be coated. And also high capital cost, slower deposition rate are the drawbacks of the PVD process.

(d) Chemical Vapor Deposition

This process involves meeting of one or more volatile precursor gases in the reaction chamber at the heated surface (substrate), and they react or decompose forming a solid phase which and are deposited onto the substrate surface.

The main steps that occur in the CVD process can be summarized as:

- Transport of reacting gaseous species to the surface.
- Adsorption of the species on the surface.
- Heterogeneous surface reaction catalyzed by the surface.
- Surface diffusion of the species to growth sites.

- Nucleation and growth of the film.

- Desorption of gaseous reaction products and transport of reaction products away from the surface [19, 20].

CVD is a more complex method of forming thin films and coatings than PVD. CVD exhibits several advantages such as the capability of producing highly pure and dense films or fine particles at reasonably high deposition rates, and the capability of coating complex-shaped components uniformly due to its non-line-of-sight nature. CVD is a versatile technique that can be used to process metallic, ceramic compound and semiconducting thin films, some of these include Elements, metals and alloys, carbides, nitrides, borides, oxides, etc., Depending on the sources used for the activation of chemical reactions, the deposition process can be categorized into thermally activated, laser-assisted and plasma-assisted CVD. The greatest problem with this technique is the associated high temperature.

(e) Thermal Spray Coatings

Thermal spray processes haven been in using to form hard coatings on selected component surface. The process involves heating of the material to be coated in a gaseous medium and projected at high velocity as molten droplets onto a substrate surface. Upon impacting the substrate surface, the droplets become flattened, transfer the heat to the cold substrate and solidify rapidly to form the 'splats'. Powders, rod and wires can be used as feedstock materials. Several processing routes can be employed depending on the materials and desired coating performances. These include plasma spraying, high velocity oxyfuel (HVOF) spraying, detonation flame spraying, and flame spraying. Metals, polymers and ceramics are the most widely used coating materials. Typical coating thickness obtainable with this process are 50-300 μm. Out of all the coating techniques Electrodeposition is the oldest and widely using technique to produce thin films the reasons were explained in detail in the coming section.

2.3 Electrodeposition

Electrodeposition is also called "electroplating", a short version of electrolytic deposition. It's a process using electrical current to reduce cations of a desired material from a solution and coat that material as a thin film onto a conductive substrate surface.

Electrodeposition is a versatile technique in making coatings, bulk products in micro to nano dimensions. Electrolyte in the electroplating process is used as precursor for the material to be developed and the material on which the material is to be deposited is termed as a cathode. If coating is the objective of the processing, then the substrate material itself is used as a cathode. Bath composition, temperature, pH, type of power supply, current density are the key parameters which influences the deposition process and hence the properties of the deposited materials. The Figure 2.1 shows a simple electroplating system for copper deposition from copper sulfate solution.
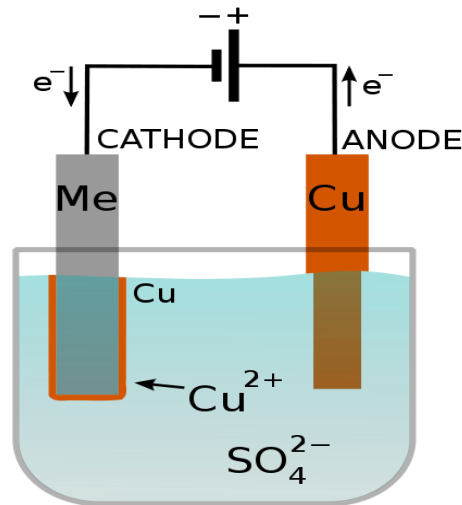
Figure 2.1: Electrodeposition setup for Copper from Copper sulfate solution.

Materials processed via electrodeposition are pure Ni, Ni-based nanocomposites, copper, Cu-based nanocomposites, layered Cu–Ni nanocomposites, pure cobalt, Co–Ni alloys, WC-based coatings, TiO_2–Ni nanocomposite coatings [2, 21] etc.

2.3.1 Advantages of Electrodeposition

Electrodeposition has several advantages over the conventional and latest deposition processes summarized as

- Low cost and industrial applicability, as it involves little modification of existing electroplating technologies.
- The process parameters can be easily tailored to get the desired microstructure.

- Simple operation, as the electro deposition parameters can be easily tailored to meet the required crystal grain size, microstructure and chemistry of products.

- Versatility, as the process can produce a wide variety of pore free materials and coatings.

- High production rates, even nano crystalline deposits can be formed on a cathode surface during plating by properly controlling the electro deposition parameters, e.g. bath composition, current density, temperature, pH, etc.,

- Process can also be operated at room temperature and pressure.

- Ability to produce compositions unattainable by other techniques.

- No post deposition treatment.

- Metals, alloys and polymers can be deposited by using this process. The metals have been deposited are Ni, Cu, Cr, Co, Au, Zn, Pd etc., and alloys such as Co-Cu, Ni-Co, Ni-Cu, Cu-Al, etc. Multilayer deposition can also be done by this process.

2.3.2 Applications of Electrodeposition

Since its invention in 1805 by Italian chemist, Luigi Brugnatelli, electroplating has become an extensively used industry coating technology. Its applications are as given below [2, 4].

1. Decoration: Coating a more expensive metal onto a base metal surface in order to improve the appearance. Applications are jewellery, furniture fittings, builder's hardware and tableware.

2. Protection: Corrosion-resistant coatings such as chromium plating of automobile parts and domestic appliances, zinc and cadmium plating of nuts, screws and electrical components. Wear-resistant coatings such as nickel or chromium plating of bearing surfaces and worn shafts.

3. Electroforming: Manufacture of sieves, screens, dry shaver heads, record stampers, moulds, and dies.

4. Enhancement: coatings with improved electrical and thermal conductivity, solderability, reflectivity etc.

5. The magnetic and electrical properties make electrodeposited nanomaterials attractive as soft magnets for high-efficiency transformers, power supplies and motor applications.

6. The exceptional catalytic properties make them strong contenders for different applications such as electrodes for hydrogen evolution and fuel cells.

2.3.3 Electrodeposition as synthesis of Nanostructured materials

Nanostructured materials are those in which the main structural dimensions vary at the nanometer scale; typical dimensions are smaller than 100 nm. From the synthesis point of view electrodeposition is one of the oldest methods used to produce nanostructured materials for many years. The synthesis of nanostructured materials with grain size control during the electrodeposition process can be considered a distinct form of grain boundary engineering in which the grain boundary content (types and quantities of grain boundaries) of a material are controlled during material processing to achieve certain physical, chemical and mechanical properties [22]. The final result is thus a bulk interfacial material, as originally defined by Gleiter [23] which does not require any further processing of precursor powder material. In this respect, electrodeposited nanocrystals are quite different from other nanostructures which are based on consolidated particles. Potentially there are a very large number of pure metals, alloys, composites, and ceramics which can be electrodeposited with grain sizes less than 100 nm. These materials can be deposited as thin films (1 to 100 µm) or in bulk form (several mm thick). The co-deposition of ceramic materials with metals and polymers has created opportunities for the preparation of novel hybrid nanomaterials and nanostructures that cannot be obtained by other methods.

Fundamentally, electrodeposition process yields grain sizes in the nanocrystalline range when the electrodeposition variables (example bath composition, *pH*, temperature, current density, etc.) are chosen such that nucleation of new grains is favored rather than the growth of existing grains. In practice, this can be achieved by using high deposition rates, formation of appropriate complexes in the bath, addition of suitable surface active elements (Surfactant) to reduce surface diffusion of ad-atoms, etc., The two key mechanisms that have been identified as the major rate determining steps for nanocrystal formation are charge transfer at the electrode surface and surface diffusion of adions on the crystal surface [24]. The diffusion of adions on the surface is controlled by inhibition, for example, it is achieved by adsorption of foreign species such as grain refiners on the growing surface. The effectiveness of the grain refiners depending upon surface adsorption characteristics, compatibility with the electrolyte and temperature stability.

For example saccharin [25], coumarin, and formic acid [26] have all been successfully applied to achieve grain refinement down to the nanocrystalline range for nickel electrodeposits. The second important factor in nanocrystal formation during electro crystallization is overpotential [27, 28]. At lower potential and high surface diffusion rates the grain growth is favored, on the other hand, high over potentials and low diffusion rates promote the formation of new nuclei.

The electrochemical processing have been used for the synthesis of nanocrystalline pure metals (e.g., Ni, Co, Pd and Cu), binary alloys (e.g., Ni-P, Ni-Fe, Zn-Ni, Pd-Fe and Co-W), and ternary alloys (e.g., Ni-Fe-Cr). Even multilayered structures or compositionally modulated alloys (e.g., Cu-Pb, Cu-Ni, Ag-Pd, Ni-P), metal matrix composites (e.g., Ni-SiC), ceramics (e.g., ZrO_2), and ceramic nanocomposites (e.g., $Tl_aPb_bO_c$) [4, 22, 29-30] have been successfully produced by electrodeposition methods. DC electroplating, pulsed-current electrodeposition, as well as codeposition processes to produce nano-composite materials are the types of electrodeposition techniques have been used to produce nanostructured materials.

2.4 Pulsed Electrodeposition

Electrodeposition is the traditional method of DC electroplating. This has been modified by the use of current interruption or even current reversal termed as pulsed electro deposition. In DC plating, only the current or potential can be varied [31]. However, in pulse plating it is possible to vary parameters independently, the current density, pulse frequency and the duty cycle which is the ratio of pulse on time to the sum of on time and off time. The properties can be improved because it is possible to obtain coherent, non dendritic deposits at much higher current densities than with the straight direct currents [31-32]. The accompanying higher over potentials results in higher nucleation rates thus results in finer grain size. Because of foreign substances may be either adsorbed or not when the current is off during pulse plating [33-34] the mechanical properties, the structure and texture can be different from those observed with conventional deposition. The important parameters of EPD process include conditions of both the electrochemical bath and the substrate. The conditions of the electrolyte bath are bath composition, temperature, current density at the cathode, and transport behavior and those of substrate (cathode) are crystallography and surface topography.

A major limitation of the electrodeposits produced by direct current is porosity and rough deposits [35]. Pulse plating improves the deposit properties viz., porosity, ductility, hardness,

electrical conductivity, plating thickness distribution, finer grain size. Numerous NC metals and alloys including Ni, Co, Cu, Zn and Ni–Fe [31-34] have been produced by pulse electrodeposition and reported to have unique properties in contrast to their coarse-grained (CG) counterparts.

2.5 Electrophoretic deposition

Electrophoretic deposition is the process of depositing charged powder particles dispersed or suspended in the liquid medium on the conductive substrate of opposite charge by the application of DC Electricfield. Compared to other advanced shaping techniques, the EPD process is versatile since it can be modified easily for a specific application. For example, deposition can be made on flat, cylindrical or any other shaped substrate with only minor change in electrode design and positioning. Also has advantages of short formation time, needs simple apparatus, little restriction of the shape of substrates. The basic difference between an electrophoretic deposition process (EPD) and an electrolytic deposition process (ELD) is that the former is based on the suspension of particles in a solvent whereas the later is based on solution of salts, i.e., ionic species [36].

The electrophoretic deposition (EPD) technique has a wide range of novel applications in the processing of advanced ceramic materials and coatings, such as in the fabrication of wear resistant and anti-oxidant ceramic coatings, fabrication of functional films for advanced microelectronic devices and solid oxide fuel cells as well as in the development of novel composites or bioactive coatings for medical implants, there has been increased interest for its application in nanoscale assembly for advanced functional materials. And also has been used successfully for thick film of silica, nanosize zeolite membrane, hydroxyapatite coating on metal substrate for biomedical applications, luminescent materials, high-Tc superconducting films, gas diffusion electrodes and sensors, multi-layer composites, glass and ceramic matrix composites by infiltration of ceramic particles onto fibre fabrics, oxide nanorods, carbon nanotube film, functionally graded ceramics, layered ceramics, piezoelectric materials [36-42], etc.,

2.5.1 Factors influencing EPD

The process being involved the deposition of charged particles from the suspension onto the conducting substrate (cathode) by the application of electric field. Thus two groups of parameters determines the characteristics of this process

(1) Parameters those related to the suspension such as Particle size, Dielectric constant of the liquid, conductivity, stability & viscosity of the suspension and Zeta potential.

(2) Parameters those related to the process including the physical parameters such as the electrical nature of the electrodes, the electrical conditions (voltage/intensity relationship, deposition time, etc.), effect of deposition time, applied voltage, concentration of the solid in the suspension.

2.5.2 Zeta Potential and its importance

Zeta potential is the electrical potential that exists at the interface between the particle surface and the stationary layer of the fluid attached to the particle; it is the key factor in the electrophoretic and electrocodeposition procesess. It is a function of surface charge of a particle, any adsorbed layer at the interface and nature and the composition of the surrounding medium in which the particle is suspended. It is a very good index of the magnitude of the electrostatic repulsive interaction between particles. It gives the degree of stability of the suspension.

If all the particles in suspension have a large negative or positive zeta potential then they will tend to repel each other and there is no tendency to flocculate. However, if the particles have low zeta potential values then there is no force to prevent the particles coming together and flocculating. The general dividing line between stable and unstable suspensions is generally taken at either +30 mV or -30 mV. Particles with zeta potentials more positive than +30 mV or more negative than -30 mV are normally considered stable.

The most important factor that affects zeta potential is *pH* of the suspension. Let us suppose that a particle in suspension with a negative zeta potential. If more alkali is added to this suspension then the particles will tend to acquire a more negative charge which indicates lower *pH* value. If acid is then added to this suspension a point will be reached where the negative charge is neutralized. Any further addition of acid can cause a buildup of positive charge, indicates the increase in the *pH*. Therefore a zeta potential versus *pH* curve will be positive at low *pH* and lower or negative at high *pH*.

The below Figure 2.2 shows the plot between *pH* versus zeta potential, the point where the curve passes through zero zeta potential is called the Isoelectric point and is very important from a practical consideration. It is normally the point where the colloidal system is least stable or the particle or molecule in the suspension carriers no net charge. In the typical schematic below the Isoelectric point (I.P) is observed at *pH* 5.5.
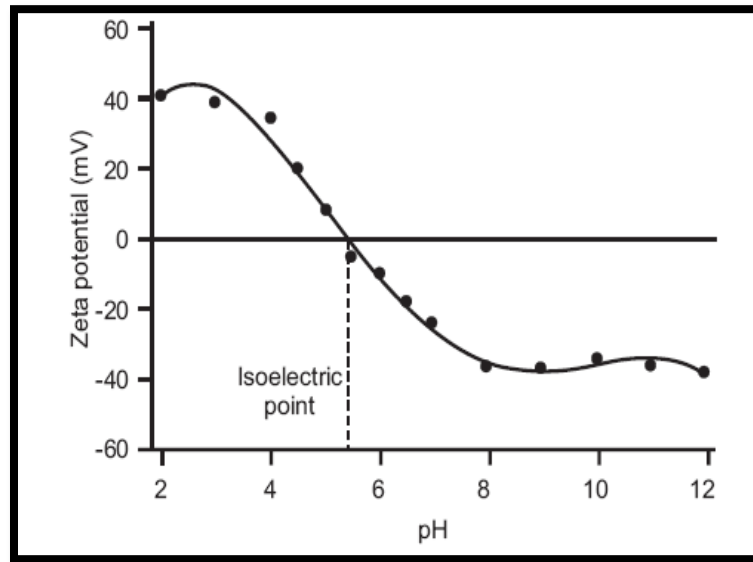
Figure 2.2: *pH* versus zeta potential illustrating the Isoelectric point.

2.6 Electrocodeposition

It is the process of particle incorporation during the electrolytic deposition of metal, which involves both the processes, elctrodeposition of metal from electrolyte solution and electrophoretic deposition of the small sized particles from the suspension, the schematic of the process is as shown in below Figure 2.3
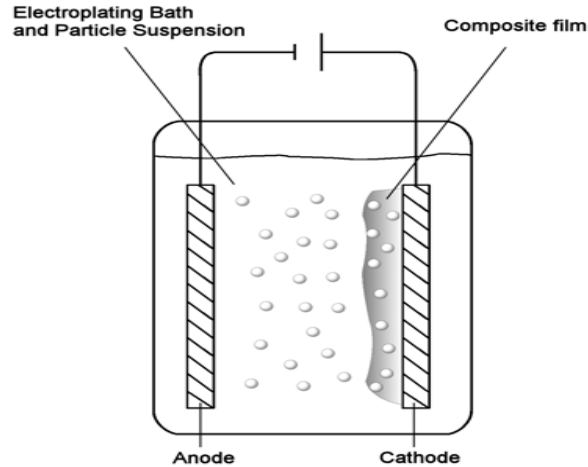
Figure 2.3: Schematic of Electrocodeposition process

This process produces composite films consisting of a metallic matrix containing a dispersion of small particles. The particles of pure metals, ceramics, and organic materials, for example oxide or carbide particles, such as Al_2O_3, SiC, TiO_2, WC, SiO_2 or diamond, a solid lubricant, such as PTFE, graphite or MoS_2, or even liquid-containing microcapsules ranging in size from sub-micron to 100 μm in diameter are used as dispersed second phase particles, and embedded in electroplated Cu, Ni, Co, Cr, and various alloys. The concentration of particles suspended in solution have varied from 2 up to 200 g/l producing composites with typically 1 to 10 vol% of embedded particles [43].

The advantages of electrocodeposition technique over other coating methods are the uniformity of deposition even for complex shapes, reduction of waste often encountered in dipping or spraying techniques, low levels of contamination, the ability to produce functionally-gradient material and to continuously process parts. In addition, this process avoids the problems associated with high temperature and high pressure processing.

The applications of these electrocodeposited coatings include wear and abrasion resistant surfaces, lubrication, high hardness tools, dispersion-strengthened alloys, and for protection against oxidation and hot corrosion [44-46]. And also Electrocodeposition has been used to produce high surface area cathodes which have been used as electro catalysts for hydrogen electrodes in industrial water electrolysis [43]. The first application of electrodeposited composite coating was the Ni/SiC coating used as the wear-resistant improvement in the Wankel engine by Metzger et al., in 1970 [47]. The metal matrix composites have been synthesized using Electrocodeposition include Ni-SiC and Ni–Co/Al_2O_3, Ni-TiO_2, Ni-Co, Ni-Zn, Ni-Fe, Co-

W, Co-P, Pd-Ni, Cu-TiO$_2$, Cu-Al$_2$O$_3$, Cu- ZrO$_2$, Cu-ZrB$_2$, Cu/CNTs, , Cu- WC, Ni-Fe-nano-Si$_3$N$_4$, Co-Ni-nano- Al$_2$O$_3$, Zn-Ni-nano-SiC etc. [43].

2.6.1 Mechanisms in Electrochemical Codeposition

The general mechanism of electrocodeposition was analogous to that of electrophoretic deposition. In electrophoretic deposition, the following steps involves in the deposition of particles from the suspension, i) the particles in suspension acquire a surface charge, ii) the charged particles are transported through the liquid by the application of an electric field (electrophoresis), iii) the particles are deposited onto the electrode, and iv) the particles adhere to the electrode surface through vander Waals forces, chemical bonding, or other forces. But the process mechanism for electrocodeposition differ from the above listed steps only in the last two steps, in which metal plating takes place simultaneously with particle deposition and metal encapsulation provides an additional means of particle adherence.

Several theoretical models have been proposed to describe the mechanism of particle entrapment of electrocodeposition process. All these theories are developed based on the investigations of micron sized particles. In 1972 Guglielmi [48] proposed the first mechanism on electrocodeposition of inert particles in the metal matrix, and later this mechanism has been adopted by various authors. According to this mechanism the process involves a two step mechanism. The solid particles are surrounded with a cloud of adsorbed ions in the electrolyte solution, and in the first step, when the particles approach the cathode they become weakly adsorbed at the cathode surface by Vander Waals forces. In the second step, particles adsorb strongly on the cathode surface by Coulomb forces and consequently are incorporated into the growing metal matrix. The model proposed by Guglielmi does not consider mass transfer.

Martin and Williams suggested that electrocodeposition was simply due to the "mechanical entrapment" of the particles by the deposited metal. Snaith and Groves [49] supported this proposition based on their observation that when a codeposited film was mechanically polished and then etched, the particles which had been incorporated within the metal matrix fell out.

A generally accepted mechanism suggested by Kurozaki [50] includes the transport of solid particles from the solution to the cathode surface by agitation. This model involves a three step process according to which, dispersed particles are transported to the Helmholtz's double layer by mechanical agitation in the first step, and in the second step, particles charged in the high

potential gradient are transported to the cathode surface by electrophoresis. In the third step, particles are adsorbed at the cathode surface by the Coulomb force which exist between particles and adsorbed anions, and are incorporated by the growing metals.

Figure 2.4 shows the common processes involved in the codeposition of particles into growing metallic layers. Five consecutive steps during the codeposition process can be identified [51]:

- formation of ionic clouds on the particles
- convection towards the cathode
- diffusion through a hydrodynamic boundary layer
- diffusion through a concentration boundary layer and finally
- adsorption at the cathode where particles are entrapped within the metal deposit.
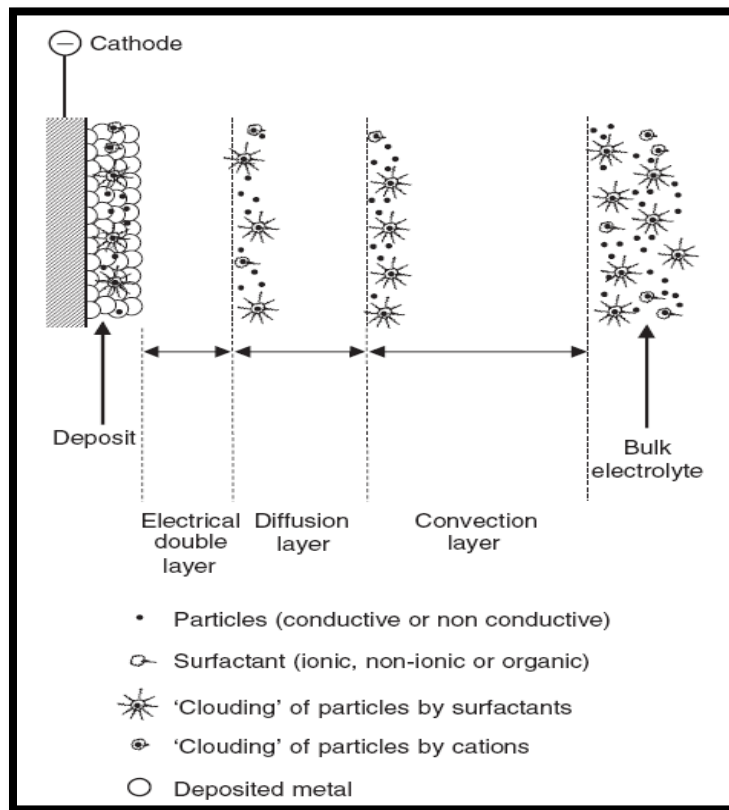
Figure 2.4: Mechanism of Particle codeposition into a metal deposit.

2.6.2 Effect of deposition parameters on ECD

(a) Bath composition

The composition of the codeposition bath is not only defined by the concentration and type of electrolyte used for depositing the matrix metal, but also by the particle loading in suspension, the *pH*, the temperature, and the additives used. A variety of electrolytes have been used for the electrocodeposition process to form metal matrix of copper include acid copper sulfate bath, alkaline pyrophosphate bath. Electrolyte concentrations typically range between 100-600 g/l and the particle loading in suspension has ranged from 2-200 g/l. The effect of some of the process variables can also vary for particle-electrolyte combinations and cell configurations.

(b) Particle Loading in Suspension

Particle loading or concentration of particles in the suspension is important factor which affects the amount of particle concentration in the deposits. At low loadings, codeposition is limited by the supply of particles to the electrode surfaces (cathode) leads to small amount of particles in the deposition. As the particle loading increases, supply of particles to the electrode increase so does the incorporation level in the deposition increases. But at the highest loadings (beyond which particle settling becomes significant), the increase in incorporation is not proportional to the increase in loading. For the parallel plate system, the amount of incorporation has been found to increase with increasing particle loading following a Langmuir-adsorption type isotherm [52].

(c) Bath Agitation

Increase in the bath agitation in the parallel plate electrode setup has been found to increase the amount of particles codeposited within the electroplated film for the Ni-Al$_2$O$_3$ and Ni-TiO$_2$ systems [53]. When the agitation is increases, a greater number of particles arrive at the electrode surface and the amount of particle incorporation in the metal film increases. However, if the agitation is too intense, the residence time for the particles at the electrode surface is insufficient and the particles are swept away before they can be incorporated into the growing metal film. Also, the amount of codeposition has also been observed to decrease in the Cu-SiC and Cu-CrB$_2$ systems with increasing agitation [54].

(d) Surfactant

The codeposition of particles increases with increasing the concentration of surfactant in the solution, this is due to the modification of the surface charge of the particles in the suspension by the absorbed molecules or ions, thereby decreasing agglomeration of particles and promoting the electrophoretic migration of the suspended particles. Thus increases in the amount of particle concentration in the film with homogenous distribution.

(e) Current Density

Current density plays an important role in controlling the deposition rate which will in turn affect the concentration of incorporated particles in the coatings. It also influences the thickness of the composite films, such that as the current density increases the thickness of the coatings increases. When the current density is increased, the amount of particle incorporation obtained has been found to increase for the Ni-TiO$_2$ system with a relatively slow agitation [54], decrease for natural or synthetic diamond in Ni [55] and for Cr particles codeposited in Ni [55] and to be unaffected when codepositing alumina in Ni. It also plays a role in the thickness of the deposited films.

(f) Particle Characteristics

Particles can be characterized by their composition and crystallographic phase, as well as by their size, density, and shape. The particle composition can have a dramatic impact on the amount of incorporation obtained for a particular bath composition. For instance three times more TiO$_2$ than Al$_2$O$_3$ has reportedly [53] been incorporated into a Ni matrix, under the same deposition conditions. The particle size also effects on the amount of codeposited particles in the composite coatings. For example when the particle size in the electrolyte increases then amount of adsorbed ions on the surface increases, which leads to the increase in the migration velocity of the particles and also results in a higher columbic force of attraction, leads to increase in the amount of the particles. But the density of particles in the coating decreases as the particle size in the electrolyte increases. For example increasing the particle size resulted in an increase in the amount of incorporation for Ni-Al$_2$O$_3$, Ni-SiC, Ni-Cr, Cu-P, and Cu-Al$_2$O$_3$ [43]. However, other researchers found particle size to have a negligible influence on the amount of incorporation for Ni-Al$_2$O$_3$ and SnNi-SiC [43].

2.6.3 Different baths used for Copper Elecetroplating

The most commonly used different plating baths for copper electrodeposition for different application purpose are Copper Cyanide plating baths, Copper pyrophosphate plating baths, and copper sulfate plating baths.

Copper cyanide plating baths typically contain 30 g/l (4.0 oz/gal) of copper cyanide and either 59 g/l (7.8 oz/gal) of potassium cyanide or 48 g/l (6.4 oz/gal) of sodium cyanide. Cathode efficiencies range from 30 to 60 percent. These baths mainly used widely in many plating operations as a strike.

Copper pyrophosphate plating baths typically contain 53 to 84 g/l (7.0 to 11.2 oz/gal) of copper pyrophosphate and 200 to 350 g/l (27 to 47 oz/gal) of potassium pyrophosphate. These baths are used for plating on plastics and printed circuits, requires more control and maintenance of the plating baths than copper cyanide plating does. However, copper pyrophosphate solutions are relatively nontoxic.

Copper sulfate plating baths typically contain 195 to 248 g/l (26 to 33 oz/gal) of copper sulfate and 11 to 75 g/l (1.5 to 10 oz/gal) of sulfuric acid. These types of baths are more economical to prepare and operate than copper pyrophosphate baths, are used for plating printed circuits, electronics, rotogravure, and plastics, and for electroforming and decorative uses.

2.7 Brief literature review on Cu-TiO$_2$ and Cu-Al$_2$O$_3$ systems

2.7.1 Cu-TiO$_2$ Literature

Catalina *et al*. prepared Cu- TiO$_2$ nano composite coating on a copper substrate using electro codeposition technique from copper sulfate bath. They studied the influence of the concentration of TiO$_2$ nano particles as dispersed phase in copper matrix coatings obtained at different current densities, and also studied the influence of TiO$_2$ on structure and properties of coatings. They have taken concentrations of nano-TiO$_2$ particles (17 nm) as 5, 10 and 50 g/l in electroplating bath. The surface morphology and composition of layers were studied by optical and scanning electron microscopy (SEM) and EDX analysis [48].

Ramalingam *et al*. prepared Cu- TiO$_2$ nano composite coating on copper substrate using electro codeposition technique from copper sulfate bath. Aim of their work was how to assess the effect of nano sized TiO$_2$ content on the wear and corrosion resistance of the deposited coatings. And

how the composition of codeposited TiO_2 nanoparticles in the composite coatings was controlled by the addition of different concentrations of TiO_2 nano particles in the bath solution. The surface morphology and composition of the nano composites were examined by scanning electron microscopy and energy dispersive X-ray spectroscopy analysis [56].

2.7.2 Cu-Al$_2$O$_3$ Literature

Andreas Bund *et al.* prepared Cu- Al_2O_3 thin films by using three different types of baths such as an acidic copper sulfate, a neutral pyrophosphate, and an alkaline sorbitol based bath, with covering a wide *pH* range were used. The highest amount of incorporated particles (ca.11 wt% alumina) was found for the pyrophosphate bath. And they measured the zeta potential of the particles in dilute solutions of the components of the plating baths. Furthermore, the microstructure, microhardness and electric conductivity of the layers were characterized [57].

I. Zamblau, *et al.* prepared Composite coatings of copper incorporating Al_2O_3 nanoparticles by using electrodeposition on carbon steel and characterized. By using electrochemical methods such as open circuit potential (ocp) measurements, polarization curves and electrochemical impedance spectroscopy, the corrosion behavior of the Al_2O_3-copper nanocomposite coatings was examined [58].

J. R. Roos, *et al*. prepared Cu-Al_2O_3 deposits containing either α-Al_2O_3 or γ-Al_2O_3 particles in copper sulphate plating baths to which the addition agents thallium sulfate or aluminum sulfate were added. In their work they studied the effect of thermo mechanical processing on the microhardness of copper deposits containing a dispersion of α-Al_2O_3 or γ-Al_2O_3 particles in the bath. The as-deposited microhardness and the effect of annealing on the microhardness and on the microstructure of cold-rolled and hot-rolled Cu- Al_2O_3 deposits were investigated in particular. The effect on mechanical properties of the use of promoting agents for codeposition was also studied [59].

2.8 Wear & Various wear Mechanisms

Wear is defined as the erosion of material from a solid surface by the action of another surface. It is related to surface interactions and more specifically the removal of material from a surface as a result of mechanical action. The real area of contact between two solid surfaces compared with the apparent area of contact is invariably very small, being limited to points of contact between surface asperities. The load applied to the surfaces will be transferred through these points of contact and the localized forces can be very large. The material intrinsic surface properties such as hardness, strength, ductility, work hardening etc. are very important factors for wear resistance, but other factors like surface finish, lubrication, load, speed, corrosion, temperature and properties of the opposing surface etc. are also equally important. Temperature has an effect on the wear rate (rate at which a material deteriorates under frictional forces) because friction generates heat, which in turn can affect the microstructure of the material and make it more susceptible.

The various types of wear are

(a) Adhesive wear

(b) Abrasive wear

(c) Erosive wear

(d) Corrosive wear

(e) Surface fatigue wear

(f) Fretting wear

(a) Adhesive wear

Adhesive wear is due to the localized bonding between contacting solid surfaces leading to material transfer between the two surfaces or the loss from either surface. Adhesive wear occurs when two bodies slides over each other, or are pressed into one another, which promote material transfer between the two surfaces. However, material transfer is always present when two surfaces are aligned against each other for a certain amount of time and the cause for material transfer or wear. Adhesive wear is the most common form of wear and is commonly encountered in conjunction with lubricant failures. High hardness and low strength are desirable properties for applications requiring resistance to adhesive wear. The process is as demonstrated in the below Figure 2.5
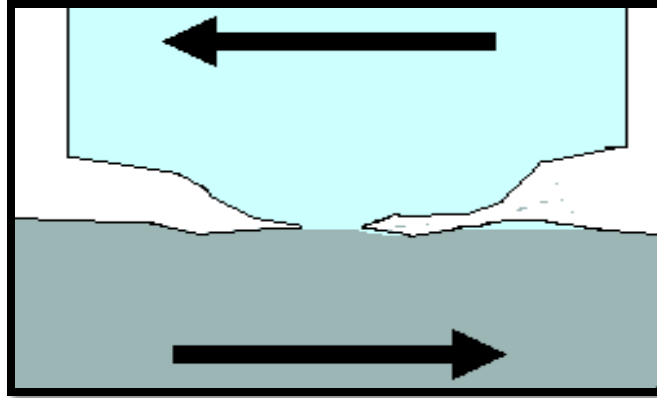
Figure 2.5: Schematic of Adhesive wear mechanism.

(b) Abrasive wear

Abrasive wear occurs when a solid surface experiences the displacement or removal of material as a result of a forceful interaction with another surface or particle. Particles can become trapped in between the two surfaces in contact, and the relative motion between them results in abrasion (displacement and removal of surface material) of the surface that has a lower hardness. Gouging, grinding, and scratching are the examples of abrasive wear. Alternatively, abrasive wear can occur in the absence of loose particles when the roughness of one surface causes abrasion and/or removal of material from the other surface. The Abrasive wear process is as demonstrated in Figure 2.6 [60].
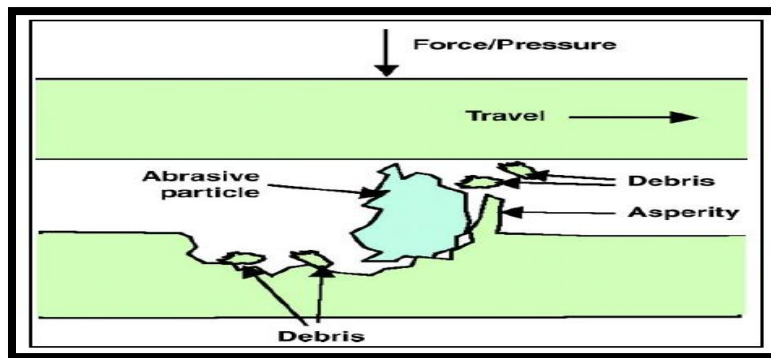
Figure 2.6: Schematic of Abrasive wear mechanism.

(c) Erosive wear

Erosive wear is caused by the impact of particles of solid or liquid against the surface of an object [61]. The impacting particles gradually remove material from the surface through repeated deformations and cutting actions [62]. The rate of erosive wear is dependent upon a number of factors. The material characteristics of the particles, such as their shape, hardness, impact velocity and impingement angle are primary factors along with the properties of the surface being eroded. The Erosive wear process is as demonstrated in Figure 2.7
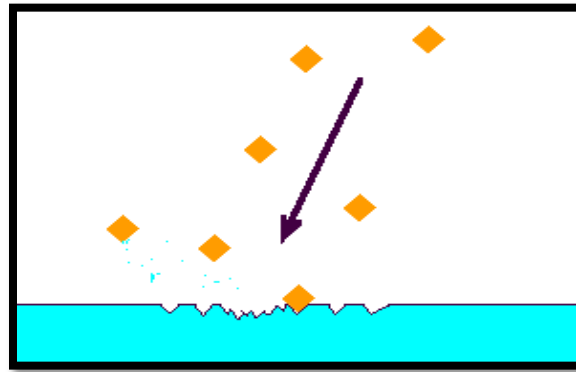
Figure 2.7: Schematic of Erosive wear mechanism.

There are three types of erosion wear

Solid particle erosion – surface wear by impingement of particles carried by a gas or fluid.
    Example*:* wear of helicopter blade leading edges in dusty environments.
Liquid drop erosion – surface wear by impingement of liquid drops.
    Example: wear of centrifugal gas compressor blades by condensate droplets.
Cavitation erosion – surface wear in a flowing liquid by the generation and implosive collapse of gas bubbles.
  Example: Cavitation erosion of a ship's propellers and of components in fluid pumps.

(d) Fretting wear

Fretting wear is due to the repeated cyclical rubbing between two surfaces, over a period of time which will remove material from one or both surfaces in contact. It occurs typically in bearings, although most bearings have their surfaces hardened to resist the problem.

(e) Corrosive wear

When the effects of corrosion and wear are combined, a more rapid degradation of the material's surface may occur. This process is known as corrosive wear. Films or coatings are often used to protect a base metal or alloy from harsh environments that would otherwise cause it to corrode.

(f) Surface fatigue wear

Surface or contact fatigue occurs when two material surfaces that are in contact with each other in a rolling or combined rolling and sliding motion create an alternating force or stress oriented in a direction normal to the surface. The contact stress initiates the formation of cracks slightly beneath the surface, which then grow back toward the surface causing pits to form as particles of the material are ejected or worn away. This form of fatigue is common in applications where an object repeatedly rolls across the surface of a material, resulting in a high concentration of stress at each point along the surface. For example, rolling-element bearings, gears, and railroad wheels commonly exhibit surface fatigue [60]. Figure 2.8 illustrates an example of the surface fatigue mechanism.
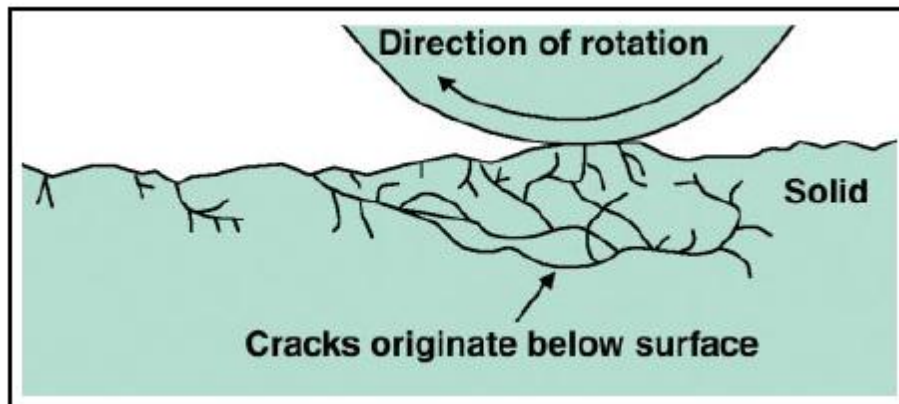
Figure 2.8: Schematic of Surface Fatigue wear mechanism.

Chapter 3

Experimental

Sample Preparation

Plating bath Solution Preparation

Particle Size Analysis

X-Ray Diffraction Studies

Microstructural Studies

Surface Mechanical Property Study

CHAPTER 3

EXPERIMENTAL

3.1 Sample preparation

For the deposition of Cu-TiO$_2$ and Cu-Al$_2$O$_3$ composite coatings, copper was selected as substrate. The substrates were collected from hot rolled copper strip by cutting it into averagely 20mm×15mm size pieces. The approximate dimensions of the substrates were 20mm×15mm×3mm. Then the substrates were mirror polished by grinding on belt grinder for oxide layer removal, then on emery papers (1/0, 2/0, 3/0, 4/0), then rough cloth polishing in which Alundum was used as abrasive agent. Finally the substrates were fine polished by fine cloth in which diamond paste was used as polishing agent. Then the substrates were cleaned with soap and then washed with water. Ultrasonication of the substrates was done for 10 minutes by using deionized water and acetone for the removal of fine particles which adsorbed on the sample surface during the polishing. In this way the mirror polished substrates were prepared for deposition. Holes were made on the samples to dip the samples in the electrolyte solution and to supply current by attaching copper wire to the hole.

3.2 Plating bath solution preparation

Parallel plate electrode configuration and Copper sulfate bath without addition of surfactant and additives, is used for the codeposition of TiO$_2$ and Al$_2$O$_3$ in the copper matrix. The bath compositions and parameters used for Cu-TiO$_2$ composite coatings are reported in the Table 3.1 and Table 3.2 respectively. As the isoelectric point of TiO$_2$ was determined around 4.2, so the *pH* of the solution maintained below this value (*pH* 2) so that the particles in the suspension acquire positive charge in the acid solution and deposited into the growing metal on cathode. Same bath compositions and plating parameters were also used for Cu –Al$_2$O$_3$ system except the *pH* value. *pH* 4 was fixed for Cu-Al$_2$O$_3$ system as no incorporation of Al$_2$O$_3$ in copper matrix at *pH* 2 was reported in the literature [43]. Pure copper strip was used as Anode and prepared copper substrates as cathodes on which composite deposition takes place. Before deposition the solution was allowed for Ultrasonication for 25minutes and magnetic stirring for 30minutes for homogenous dispersion of the TiO$_2$ powder in the solution. Magnetic stirring was also allowed

for stirring of the bath during entire deposition so that the sedimentation of powder particles in the solution is prevented and they can be homogeneously dispersed during deposition in the copper matrix. Pure copper deposits were also done by using the parameters which have used for TiO_2 deposition for comparison of the results obtained, with the results obtained by using particle incorporation. After deposition the samples were washed with distilled water, kept in the paper and preserved for Characterizations.

Table 3.1: Composition of Copper sulfate bath solution for Cu-TiO_2 / Cu- Al_2O_3 and pure copper coatings

Electrolyte (Acidic copper sulfate bath)	Copper Sulfate ($CuSO_4.5H_2O$): 200 gm/l
	Sulfuric acid (H_2SO_4): 50 gm/l
pH	2.17
Current density	5 A/dm^2, 8 A/dm^2, 11 A/dm^2 , 14 A/dm^2
Temperature	27 °C
Plating time	20 minutes
Dispersion	TiO_2 / Al_2O_3: 0 gm/l, 10 gm/l, 30 gm/l

Table 3.2: Deposition parameters of Cu-TiO_2/ Cu-Al_2O_3 and un reinforced Copper coatings

S .No	1	2	3	4	5	6	7	8	9	10	11	12
TiO_2/Al_2O_3 concentration in bath(gm/lit)	__	__	__	__	10	10	10	10	30	30	30	30
Current density(A/dm^2)	5	8	11	14	5	8	11	14	5	8	11	14

3.3 Particle size analysis

The particle size of TiO_2 and Al_2O_3 powder which were procured from Inframat Advanced Materials, Formington, USA was checked by Malvern Zetasizer nano series Nano- ZS model instrument. Before measuring the particle size, very small amount of powder particles were dispersed in deionized water and magnetic stirring was allowed for 30minutes followed by 10minutes ultrasonication for homogeneous dispersion of particles in the solution. The below Figure 3.1 shows the photograph of Malvern Zetasizer which can measure particle sizes from

nanometer size to micron size, and which can also used to measure zeta potential of suspended particle in a solution.

Figure 3.1: Nano zeta sizer (Model: Nano ZS, Malvern instrument)

The zeta potential of the particles (TiO_2 & Al_2O_3) were also measured with this Zetasizer at different *pH* values of the suspensions and the values are drawn against different *pH* values to find the isoelectric point and also to estimate the stable suspension *pH* value required for cathodic deposition of the ceramic particles.

3.4 X-ray diffraction studies

X- Ray Diffraction studies of all the deposited samples were performed by using, Philips X'Pert system with Cu K_α radiation (λ= 1.5418A°) to judge the phases formed, to calculate the crystallite sizes and also to determine the Relative Texture Coefficient (RTC) of the deposits. The same was also done for pure copper sample which was used as substrate and for raw powders of TiO_2 and Al_2O_3. The XRD was carried out with 2θ range of 20°-100° with scan rate of 3 degrees per minute.

3.5 Microstructural studies

3.5.1 Scanning Electron Microscope (SEM) studies

Scanning Electron Microscopic studies were performed to view the morphology of the coatings, distribution of the particles, to determine the composition and thickness of the coatings by using JEOL 6480 LV scanning electron microscope (SEM) equipped with an energy dispersive X-ray (EDX) detector of Oxford data reference system which is shown in the below Figure 3.2. Field effect scanning electron microscope (FESEM) of model ZEISS: SUPRA 40 was also used to determine the compositions and for high resolution micrographs of the coatings deposited.

Figure 3.2: JEOL JSM-6480LV Scanning Electron Microscopy

3.6 Surface mechanical property studies

3.6.1 Microhardness Measurement

Microhardness of the composite coatings (Cu-TiO$_2$ & Cu-Al$_2$O$_3$), pure copper coatings and the pure copper (substrate) were determined by using LECO LM700 michrohardness tester which is shown in Figure 3.3. The machine have minimum 1gf and maximum 1000 gf load, Dwell time 5-99sec and Knoop or Vickers indenter is included . The test was carried out with 10 gf load for 15 seconds to ensure that the indentation is up to the coating surface only. The hardness values were taken at 5 different places on the surfaces and average of these values were considered in the results.

Figure 3.3: LECO LM700 Microhardness tester

3.6.2 Wear Behavior of the Coatings

The sliding wear resistance of the composite coatings and pure copper coatings were evaluated by using ball on plate type wear testing instrument having a hardened steel ball (SAE 52100) indenter of 2 mm diameter. DUCOM TR-208-M1 ball on plate wear tester was used for this study to evaluate the wear resistance of all the coated samples with 500 gm load, 10rpm speed and 5minutes duration time. Graphs were plotted against Sliding distance vs. wear depth to

compare the wear resistances of the different samples. Scanning Electron Microscope (SEM) was used to analyze the surface damages caused by the wear testing machine to get an idea about the wear mechanism.

Figure 3.4: DUCOM TR-208-M1 Ball on plate wear tester

Chapter 4

Results and Discussions

Particle size

Zeta potential measurement

XRD analysis

Microstructural characterization

Surface Mechanical properties

Brief comparison of TiO_2 and Al_2O_3 systems

CHAPTER 4

RESULTS AND DISCUSSIONS

4.1 Particle Size

The below Figure 4.1 (a) & (b) shows the particle size distributions of TiO_2 and Al_2O_3 powders obtained by using Malvern Zeta sizer. From the figure it can be seen that no sharp peak was observed in both the cases, it indicates that a range of different sized particles were present in the bulk powder. In case of titania minimum size was observed at 91 nm and maximum 295 nm. But higher volume percentage of particles having sizes between 105 nm to 190 nm. From the cumulative study the mean size obtained for TiO_2 was 202 nm. In case of Alumina, the minimum size observed was 190 nm and the maximum size was 342 nm, but the higher volume percentage of particles was having sizes between 220 nm to 295 nm. The mean size obtained for Al_2O_3 was 287 nm.
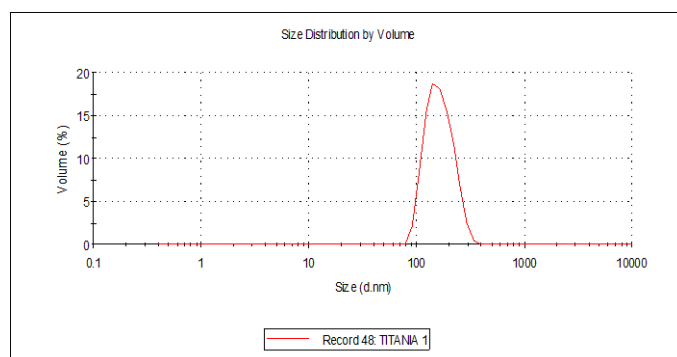
(a)
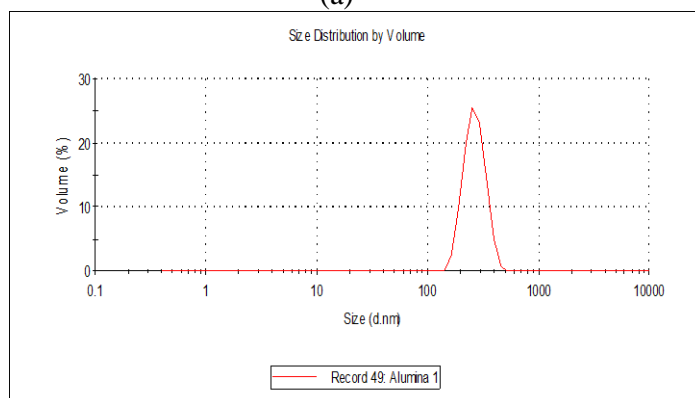
(b)

Figure 4.1: Particle size distribution of (a) TiO_2 powder (b) Al_2O_3 powder.

4.2 Zeta potential Measurement

Zeta potential of TiO_2 & Al_2O_3 ultrafine particles in de-ionized water at different *pH* values was measured to determine the iso-electric point for stable suspension by using Malvern Zetasizer nano series Nano- ZS model instrument prior to the electrodeposition. From the below Figure 4.2(a) it can be observed that the iso-electric point of TiO_2 was around 4.2 in *pH*, where as it is around 5.5 [63] according to the literature. The *pH* maintained in our case for Cu-TiO_2 system was around 2.0 *pH*, which was lower than the obtained iso-electric point *pH*, which signifies the acidic nature of the solution and the particles were positively charged in the suspension. Similarly from Figure 4.2 (b) the iso-electric point of Al_2O_3 was observed around 5.3 in *pH*, according to literature it is 8-9 [64] in *pH*. In our case for Cu-Al_2O_3 system the *pH* was maintained at 4.0 *pH*, which also signifies the acidic behavior of the solution and the particles were positively charged in the suspension.

(a)   (b)
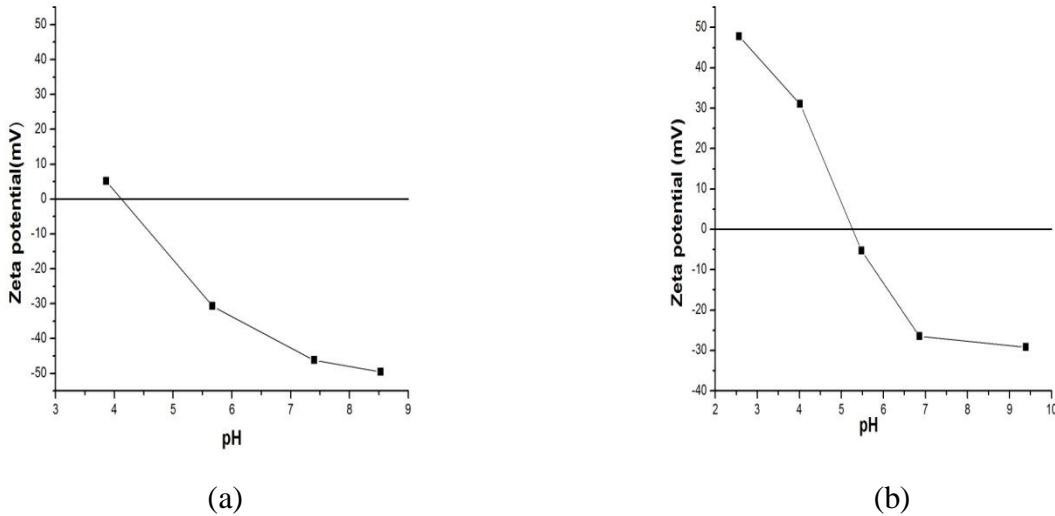
Figure 4.2: *pH* Vs Zeta potential for iso electric point determination of (a) TiO_2 (b) Al_2O_3 powder in water.

4.3 XRD Analysis

X-Ray diffractograms of Raw Powders (TiO_2 & Al_2O_3) procured from Inframat Advanced Materials, Formington, USA, all developed coatings and Pure Copper (substrate) was performed by using Philips X'Pert System. Figure 4.3(a) shows the XRD pattern of raw TiO_2 powder shows tetragonal crystal structure. But there is no appreciable peak broadening was observed though the crystallite sizes are in nanometric size. The powder source was confirmed to be synthesized by a chemical route which does not introduced any strain in the powder material. So, the broadening observed was only due to the fine crystallite size, not due to the strain.
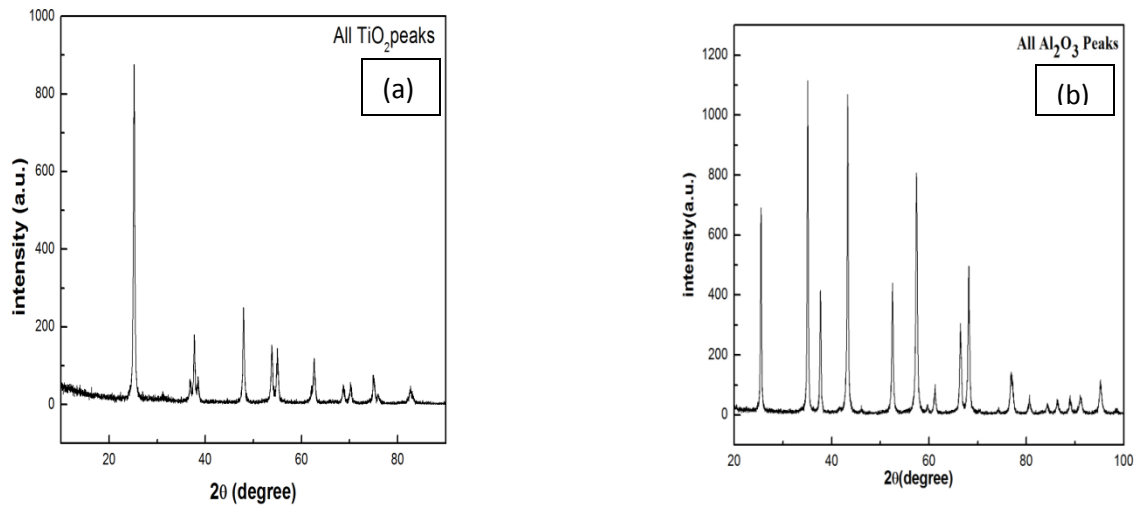
Figure 4.3: XRD peaks of (a) Raw TiO_2 powder (b) Raw Al_2O_3 powder.

Thus the XRD peaks do not show broadening though the crystallite sizes are small. Figure 4.3(b) shows the XRD peaks of Al_2O_3 Raw powder, indicating the Rhombohedra crystal structure. The features of Al_2O_3 are also same that as TiO_2 powder.

The below Figures 4.4 & 4.5 shows the comparable XRD patterns of Cu-TiO_2 and Cu-Al_2O_3 at 10 g/l, 30 g/l along with XRD pattern of substrate (pure copper). The crystallite sizes of all the coated samples were calculated by using Scherrer formula [65-66] given by equation (1) with (111) peak as reference peak and are given in below Table 4.1, 4.2 & 4.3. The crystallite sizes observed were all are less than100 nm. The Scherrer equation is given by

$$D = \frac{0.94\,\lambda}{\beta\,cos\theta} \qquad \text{----------------------- (1)}$$

Where D is the crystallite size, β is the full width at half maximum (FWHM) of the diffraction peak, λ is the wavelength of the incidental X-ray (1.54 A°) and θ is the diffraction angle.

The Relative Texture Coefficient (RTC$_{(hkl)}$) of 4 peaks namely (111), (200), (220) and (311) of all coated samples were calculated for texturing study by using below equation (2) and the results were given in below tables along with the crystallite sizes. The RTC [67-68] is defined as

$$RTC_{(hkl)} = \frac{I_{(hkl)} / I_{0\,(hkl)}}{\Sigma\,I_{(hkl)} / I_{0\,(hkl)}} \times 100\% \text{----------------------(2)}$$

Where I(hkl) is the intensity obtained from textured sample and I$_0$(hkl) is the intensity of the Standard oriented sample i.e., from JCPDS data.

The below Figure 4.4 and Table 4.1 shows the comparable XRD patterns for Cu-TiO$_2$ system for 10 g/l and 30 g/l TiO$_2$ in the bath. From the figure it is evident that all the peaks showing were belonging to the Cu. Though TiO$_2$ is present in all Cu-TiO$_2$ coated samples evidenced by the EDS compositional study but no peak of TiO$_2$ was not clearly observed because of very less intensity of TiO$_2$ peaks which is due to the higher intensity of the Cu peaks and small wt% TiO$_2$ (less than 10%) co deposited in the composite coating. The TiO$_2$ (Anatase type, JCPDS No: 84-1285) peaks were observed with very less intensity at 2θ angles of 25.24°, 48.0° degrees in Cu-TiO$_2$ coatings, to judge this only the XRD peaks of TiO$_2$ 10 g/l, 8 A/dm^2 was enlarged which is shown in Figure 4.5.

(a)　　　　　　　　　　　　　　　　　**(b)**
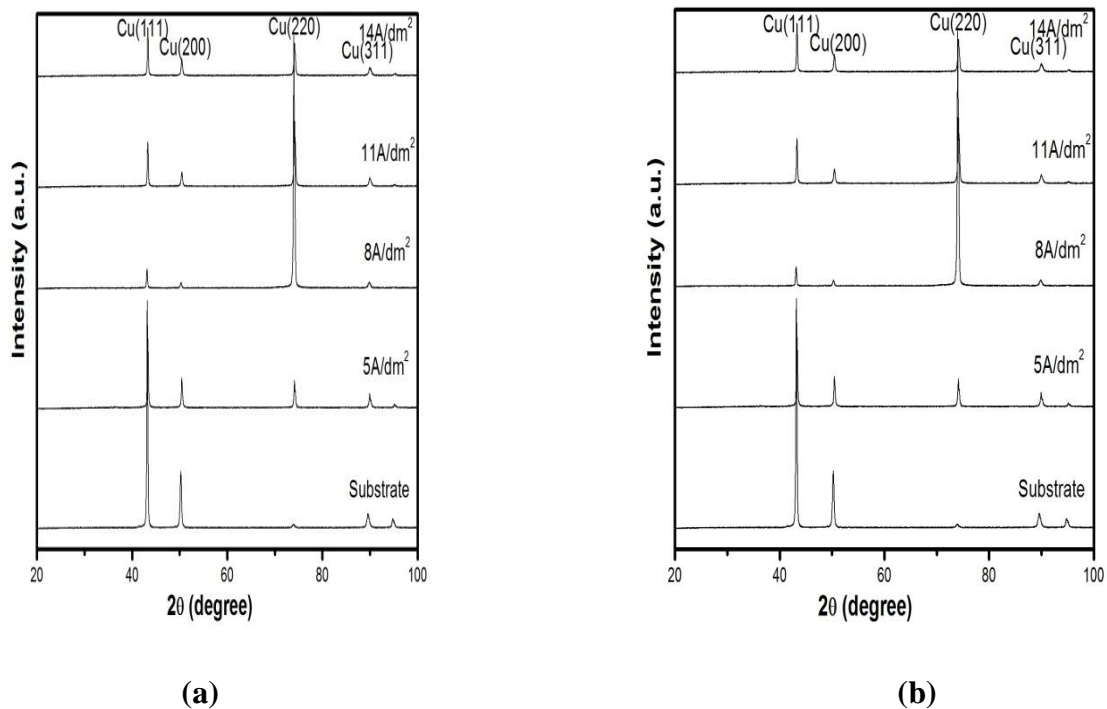
Figure 4.4: Comparable XRD pattern of Cu-TiO$_2$ coatings (a) 10 g/l TiO$_2$ (b) 30 g/l TiO$_2$ in the bath along with substrate (pure Cu) XRD pattern.
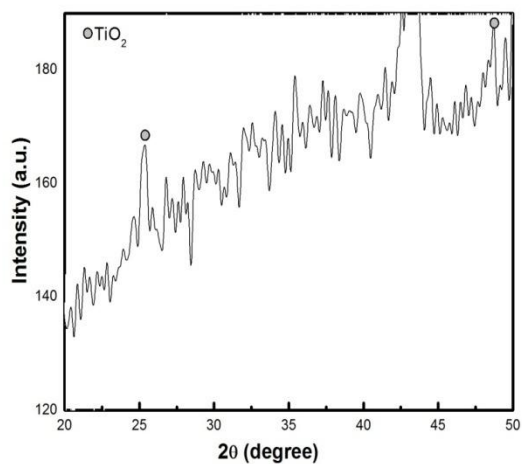
Figure 4.5: Enlarged XRD pattern of Cu-TiO$_2$ coating at TiO$_2$ 10 g/l, current density 8 A/dm^2.

Table 4.1: Relative Texture Coefficient ($RTC_{(hkl)}$) of Cu- TiO_2 composite coatings at 10, 30 g/l TiO_2 and current densities 5, 8, 11, 14 A/dm^2.

Sample details	RTC (%)				Crystallite size (nm)
	(111)	(200)	(220)	(311)	
10 g/l, 5 A/dm^2	22	13	41	24	50
10 g/l, 8 A/dm^2	3	2	88	7	65
10 g/l, 11 A/dm^2	0.2	0.2	98	1.6	57
10 g/l, 14 A/dm^2	26	22	30	22	65
30 g/l, 5 A/dm^2	20	17	40	23	65
30 g/l, 8 A/dm^2	1	1	96	2	76
30 g/l, 11 A/dm^2	9	6	75	10	51
30 g/l, 14 A/dm^2	17	11	56	16	41

From the Table 4.1, Table 4.2 & Figure 4.4 it can be observed that (220) is the most intense diffraction line (texture) in both composite coatings and pure copper deposition at all current densities except at 11A/dm^2, whereas the substrate shown a strong (111) texture. The quality of the (220) texture was obviously affected by the incorporation of particles and the current density. At 5 A/dm^2 in both of cases 10 g/l and 30 g/l the intensity of (220) is less (41%) which is accompanied by increase in the intensities of (111), (200) and (311) lines which is attributed to the higher amount of TiO_2 embedded in the coatings (Table 4.4). As the current density increased from 5 A/dm^2 to 8, 11 A/dm^2 the intensity of (220) texture increased by 47% and 57%, the increase was accompanied by decrease in the intensities of (111), (200) & (311) lines, this is due to the lower content of TiO_2 embedded in the composite coatings compare to 5A/dm^2. At 14 A/dm^2, 10 g/l the (220) texture was changed to (220)+(111) mixed preferred orientations, this might be due to higher over potential which affects the nucleation and growth of crystallites and also due to the hydrogen evolution at higher current densities.

Below Figure 4.6 and Table 4.3 shows the comparable XRD patterns of Cu-Al$_2$O$_3$ for 10 g/l and 30 g/l in the bath. From the Figure 4.6 it can be seen that (111), (200), (220), (311) and (222) peaks of Cu were present along with the peaks of Copper Oxide (Cu$_2$O, JCPDS NO: 05-0667) at 2θ angles of 29.555°, 36.419°, 42.298° and 61.369°. In pure copper & Cu-Al$_2$O$_3$ depositions (220) was the texture orientation, but the quality of (220) texture was affected by the Al$_2$O$_3$ presence in the coatings, current density and the Copper oxide similarly as Ni(OH)$_2$ in Nickel deposition[69]. From the Figure 4.6 it can be seen that the intensity of (220) texture was increased with the decrease in the intensity of copper oxide peaks at 36.419° and 61.369° as the current densities increased from 5 A/dm^2 to 14 A/dm^2.

(a)   (b)
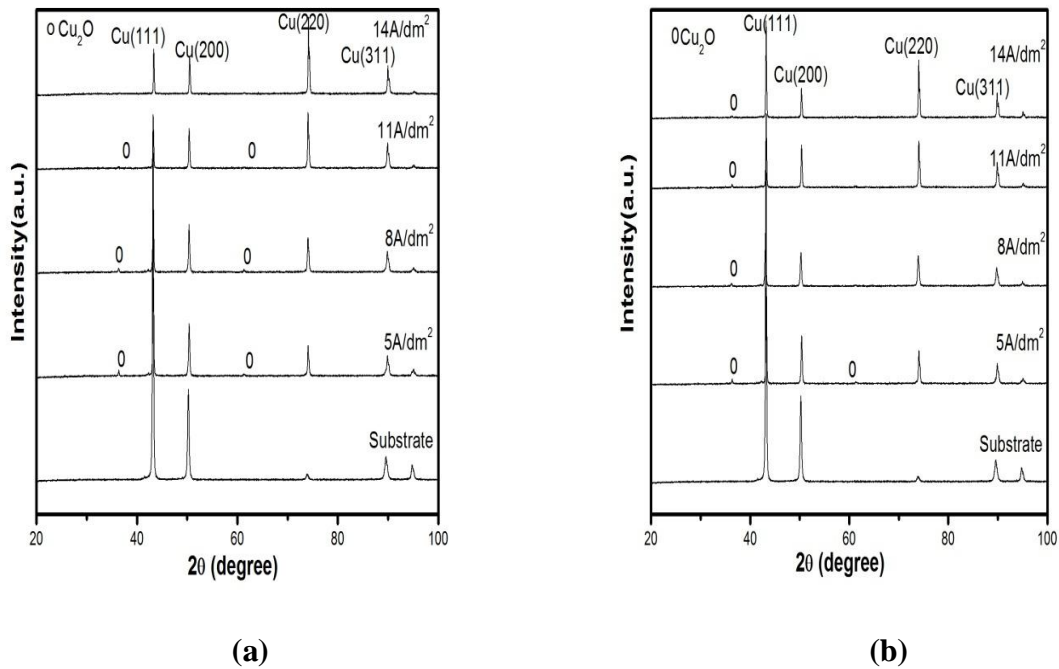
Figure 4.6: Comparable XRD pattern of Cu-Al$_2$O$_3$ coatings (a) 10 g/l Al$_2$O$_3$ (b) 30 g/l Al$_2$O$_3$ in the bath along with XRD pattern of substrate (pure Cu).

Table 4.2: Relative Texture Coefficient ($RTC_{(hkl)}$) of $Cu-Al_2O_3$ composite coatings at 10, 30 g/l Al_2O_3 and current densities 5, 8, 11, 14 A/dm^2.

Sample details	RTC (%)				Crystallite size (nm)
	(111)	(200)	(220)	(311)	
10 g/l, 5 A/dm^2	26	22	29	23	41
10 g/l, 8 A/dm2	18	21	36	25	45
10 g/l, 11 A/dm^2	9	16	48	27	50
10 g/l, 14 A/dm^2	7	12	57	24	62
30 g/l, 5 A/dm^2	20	19	37	23	53
30 g/l, 8 A/dm^2	14	19	41	26	45
30 g/l, 11 A/dm^2	14	16	43	27	64
30 g/l, 14 A/dm^2	16	11	49	24	64

At 5 A/dm^2, 10 g/l two preferred diffraction lines (220) & (111) were observed, this is attributed to higher percent of copper oxide formation. As the current density increased further to 8, 11 A/dm^2 the (220) texture changed to (220)+(311) mixed preferred orientations with (220) intensity increased by 7%, 19% respectively, this is due to the higher co deposition of Al_2O_3 and decreased intensity of copper oxide, the increase is balanced by the decrease in intensities of (111) and (200) lines. At 14 A/dm^2 less co deposition of Al_2O_3 and smaller formation of copper oxide leads to increase in (220) texture further by 28%. The similar trend was observed in case of 30 g/l Al_2O_3 in bath as observed in 10 g/l Al_2O_3 in the bath.

In the summary from the above discussions on texture study of $Cu-TiO_2$ and $Cu-Al_2O_3$ systems it can be conclude that the observed texture is due to the influence of current density, embedding second phase ceramic particles and copper oxide formation in the composite coatings.

Table 4.3: Relative Texture Coefficient ($RTC_{(hkl)}$) of unreinforced Copper coatings at current densities 5, 8, 11 and 14 A/dm^2.

Sample details	RTC (%)				Crystallite size (nm)
	(111)	(200)	(220)	(311)	
5 A/dm^2	2	1	90	7	41
8 A/dm^2	1	0.5	95	3.5	56
11 A/dm^2	51	14	19	16	53
14 A/dm^2	6	8	74	12	64

4.4 Microstructural Characterization

4.4.1 EDS Analysis

The below Figure 4.7 (a) shows the Energy Dispersive Spectrum (EDS) of Cu-TiO$_2$ coating surface prepared at 10 g/l, 5 A/dm^2, with this it is evident that Ti (0.76wt%) of particles were present in the composite coating along with copper (97.12wt%) and oxygen (2.13wt%). Similarly the Figure 4.7(b) shows the EDS of Cu-Al$_2$O$_3$ coating prepared at 30 g/l, 11 A/dm^2 which gives the evidence of presence of Al (4.69wt%) particles along with oxygen (5.96wt%) and copper (89.35wt%). Different wt% of TiO$_2$ and Al$_2$O$_3$ reported in the composite coatings depending on particle concentrations in the bath and current densities, those are given in Table 4.4 and shown in Figure 4.10
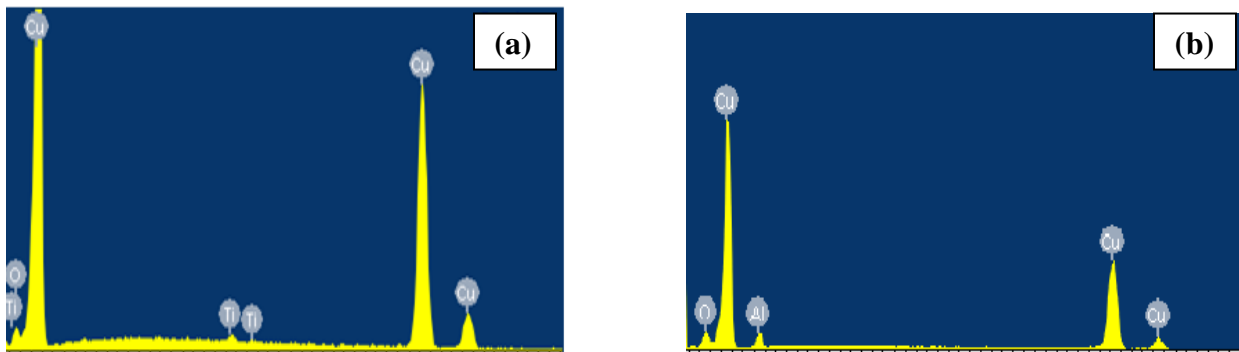
Figure 4.7: EDS of (a) Cu-TiO$_2$ deposited at 10 g/lTiO$_2$, 5 A/dm^2 (b) Cu-Al$_2$O$_3$ deposited at 30g/l Al$_2$O$_3$, 11 A/dm^2.

The below Figures 4.7 (c) & (d) shows the spot EDS on Cu-TiO$_2$ & Cu-Al$_2$O$_3$ coating surfaces particularly on the powder particles found in the coating surfaces. Such spot EDS on Cu-TiO$_2$ coatings (Fig 4.7(c)) also resulted the presence of Ti particle (2.31wt%) and Oxygen (16.90wt%) in the copper matrix. Similarly Figure 4.7 (d) shows the presence of Al (1.59wt%) and oxygen (3.14wt%) in the Cu-Al$_2$O$_3$ composite coating.
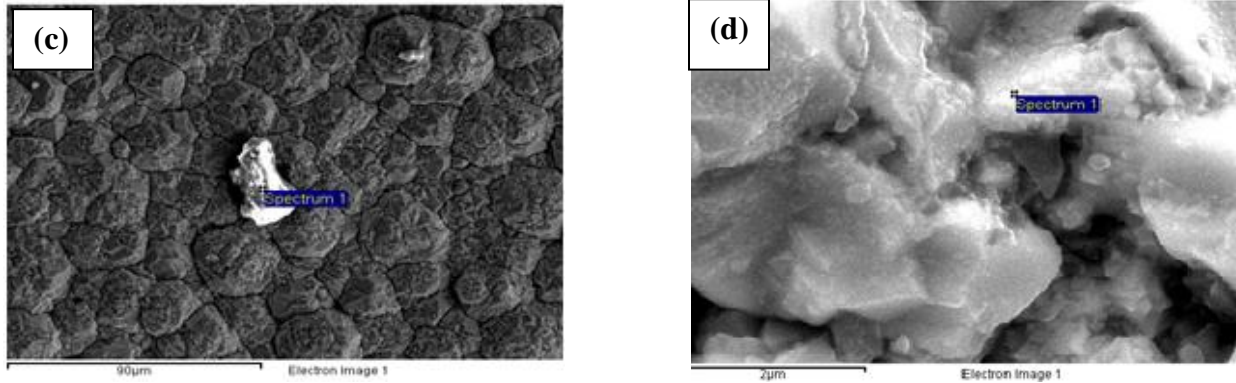
Figure 4.7: Spot EDS on surface of (c) Cu-TiO$_2$ (d) Cu-Al$_2$O$_3$ composite coatings.

Table 4.4: Co-deposited TiO$_2$ (in terms of Ti), Al$_2$O$_3$ (in terms of Al) wt% in Cu-TiO$_2$ & Cu-Al$_2$O$_3$ composite coatings at 10 g/l, 30 g/l in the bath and current densities 5, 8, 11 and 14 A/dm^2

Current density (A/dm^2)	TiO$_2$ (wt%)		Al$_2$O$_3$ (wt%)	
	10 g/l	30 g/l	10 g/l	30 g/l
5	0.76	2.59	0.59	0.95
8	0.68	0.78	0.32	4.46
11	0.70	1.51	2.21	4.69
14	0.48	1.35	0.27	0.69

4.4.2 Scanning Electron Microscope (SEM) Studies

The surface morphology and particle distribution of the electrodeposited composite coatings were performed by using SEM (JEOL JSM-6480LV) and Field Effect Scanning Electron Microscope (FESEM) of ZEISS: SUPRA 40. The below Figure 4.8 shows SEM surface micrographs of the electrodeposited Cu-TiO$_2$ composite coatings prepared at 10 g/l, 30 g/l TiO$_2$ in the bath and current densities 5 A/dm^2, 11 A/dm^2 without adding any surfactant to the bath.
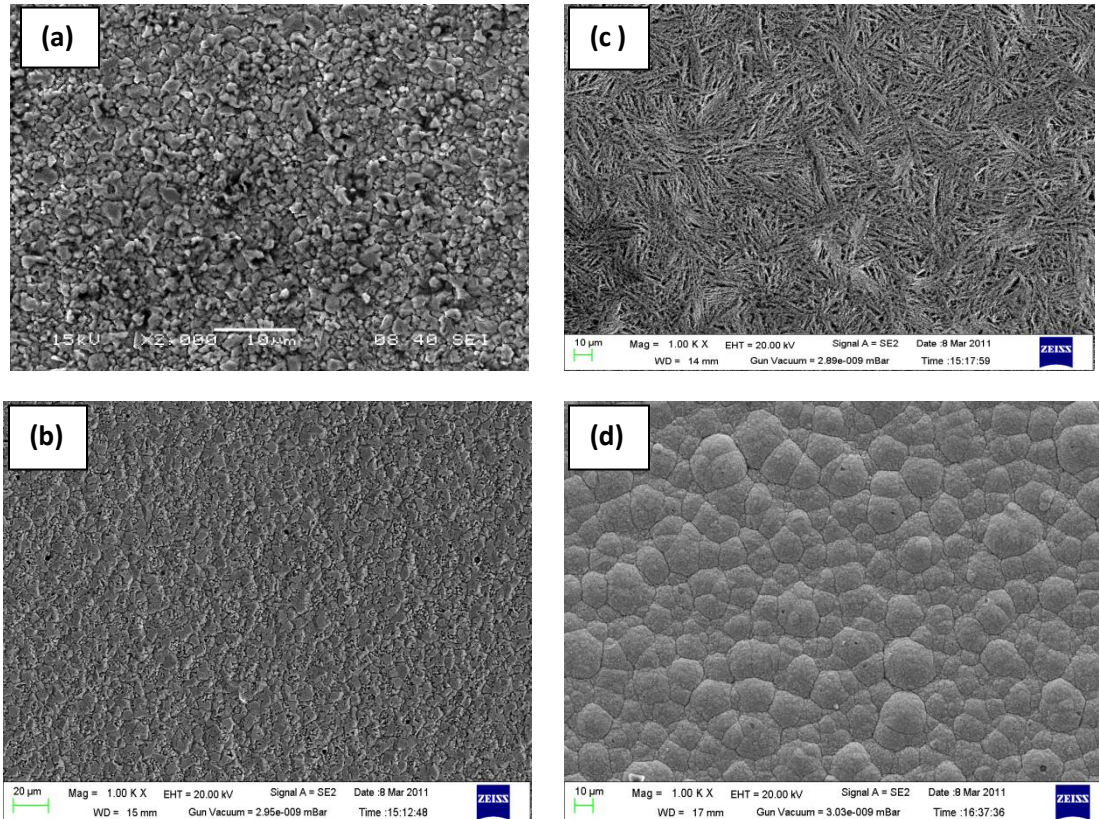
Figure 4.8: Surface morphology of electrodeposited Cu-TiO$_2$ coatings (a) & (b) TiO$_2$ 10 g/l in bath, current density 5, 11 A/dm^2, (c) & (d) TiO$_2$ 30 g/l in bath current density 5, 11 A/dm^2.

From the above Figure 4.8 it can be observed that smooth coating surfaces at all deposition conditions and also absence of nodules, cracks and dendrites like structure was observed on the coating surfaces. But the current density had greatly influenced the crystal structure of the copper matrix. As no surfactant is added to the bath, large agglomeration of the particles was observed in both Cu-TiO$_2$ and Cu-Al$_2$O$_3$ systems (Figure 4.9(f)). At 10 g/l TiO$_2$ and 5, 11 A/dm^2 current densities (Figure 4.8 (a) & (b)) the micrographs were smooth and fully compacted, but small micro pits were observed at 11 A/dm^2 current density this is attributed to evolution of hydrogen

43

at the cathode surface. At 30 g/l, 5 A/dm^2 the surface morphology of the coating observed as ropes like structure with void space and loosely compacted on the surface which is completely different microstructure compare to other micrographs of the Cu-TiO$_2$ coatings. At 30 g/l, 11 A/dm^2 the micrograph shows the cauliflower like structure that smaller grains are agglomerated and formed larger grains with well defined grain boundaries, and also grain refinement have been observed at this current density and particle concentration.

Figure 4.9 (e) & (g) shows the SEM surface morphologies of the Cu-Al$_2$O$_3$ composite coatings developed at 10 g/l, 30 g/l Al$_2$O$_3$ and current density 5 A/dm^2. At 10 g/l the powder is not distributed uniformly, some powder segregated zones can be seen where the actual crystal growth is disturbed. Similar features observed at 30 g/l, 5 A/dm^2 with bigger morphology.

Figure 4.9(f) & (h) shows the surface morphologies of Cu-Al$_2$O$_3$ coatings at 10 g/l, 30 g/l Al$_2$O$_3$ and current density 11 A/dm^2, agglomerated powder can be seen from Fig. 4.9 (f), where as the powder was distributed over all grains is observed at 30 g/l, 11 A/dm^2 current density.
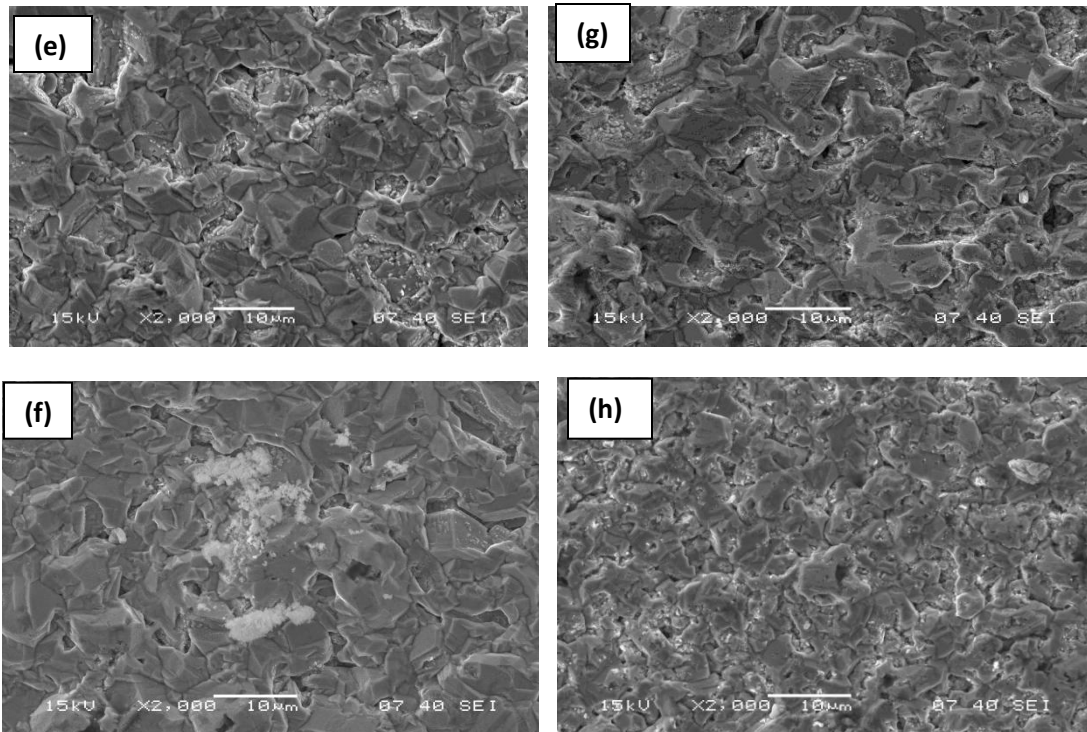
Figure 4.9: Surface morphology of electrodeposited Cu-Al$_2$O$_3$ coatings (e) & (f) Al$_2$O$_3$ 10 g/l in bath, current density 5, 11 A/dm^2 (g) & (h) Al$_2$O$_3$ 30 g/l in bath, current density 5, 11 A/dm^2.

4.5 Effect of TiO_2 & Al_2O_3 concentration in bath

The Figure 4.10 (a) & (b) shows relationship between the particle (TiO_2 & Al_2O_3) loading in the plating bath for 10 g/l, 30 g/l and the co deposited wt% of TiO_2 (in terms of Ti) and Al_2O_3 (in terms of Al) in the composite coatings at four current densities 5, 8, 11,14 A/dm^2. From the Figure 4.10(a) it can be observed that a sharp increase in the co deposited wt% of TiO_2 at all current densities as the TiO_2 loading in bath increased from 10 g/l to 30 g/l. Thus the amount of codeposited TiO_2 wt% increased in the composite coating as the amount of TiO_2 increased in the plating bath [56]. The same was reported in earlier [56]. This is due to increased amount of TiO_2 supply to the cathode region as the amount of TiO_2 increases in the plating bath. In other words, a higher concentration of TiO_2 particulates in the electrolyte enhanced the adsorption rate, thus resulting in a higher weight percentage of the codeposited TiO_2 nano-particulates in the coating. However, the increase in the amount of co-deposited titania particles is not quantitatively comparable with the amount of particles charged to the electrolyte. For example, by increasing the amount of TiO_2 from 10 to 30 g/l with three times, the particle concentration in the deposited layer was increased only 2 times. Higher amount of TiO_2 wt% observed at 5 A/dm^2 in both the cases this is evident from the EDS compositional study. The Codeposition of TiO_2 nanoparticles on the cathode surface was suggested by Guglielmi's two-step adsorption model [56].

Figure 4.10: Effect of TiO_2 /Al_2O_3 concentration in bath on co deposited wt% of (a) TiO_2 (in terms of Ti) (b) Al_2O_3 (in terms of Al) in composite coatings at current densities 5, 8, 11 and 14 A/dm^2.

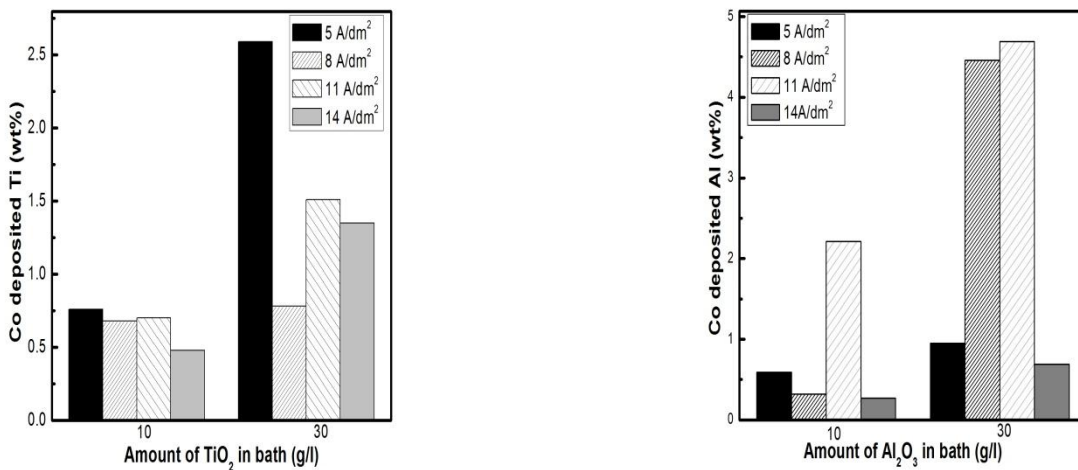According to this model in the first step the particles are loosely adsorbed on the cathode surface due to the weak vander waal forces, and in the second step the particles are strongly adsorbed on the cathode surface due to the Columbic attractive forces acting between the cathode surface and the anions adsorbed on the particles, then consequently the particles are encapsulated in the growing metal matrix.

Same features were observed in case of Cu-Al$_2$O$_3$ system also the Figure 4.10(b) demonstrates the results obtained. As the Al$_2$O$_3$ concentration in the bath increases from 10 g/l to 30 g/l the wt% of the co deposited Al$_2$O$_3$ is also increased. Higher amount of Al$_2$O$_3$ found as 4.69wt% at 30 g/l, 11 A/dm^2.

4.6 Surface Mechanical Properties

4.6.1 Microhardness study

The microhardness of the composite coatings and pure copper coatings were measured by using Leco LM700 microhardness tester by applying 10gf load for 15 seconds in order to ensure that the microhardness values are not affected by the substrate. Figures 4.11 (a) & (b) shows the effect of current density on microhardness of Cu-TiO$_2$ and Cu-Al$_2$O$_3$ composite coatings developed at current densities 5, 8, 11 and 14 A/dm^2 without addition of any surfactant and additives to the bath. Generally the strengthening mechanism of poly crystalline metals, alloys and MMCs mainly due to (a) grain refinement strengthening from Hall–Petch relationship (b) dispersion strengthening due to Orowan mechanism (c) solid solution strengthening (d) crystal orientation. In the present work the hardness values were observed are mainly depending on dispersion strengthening due to the dispersed second phase particles and preferred crystal orientation (Texture) of the matrix phase and marginal effect of grain size.

The hardness values obtained for the composite coatings (Cu-TiO$_2$ & Cu-Al$_2$O$_3$) are higher than pure copper (50HV-105HV) [70] at all current densities, also higher than the hardness values of substrate (pure copper) 95.1HV and un reinforced copper coatings (83.3 HV to 129.9 HV). This is attributed to the dispersion strengthening caused by the dispersed second phase particles in the composite coatings.
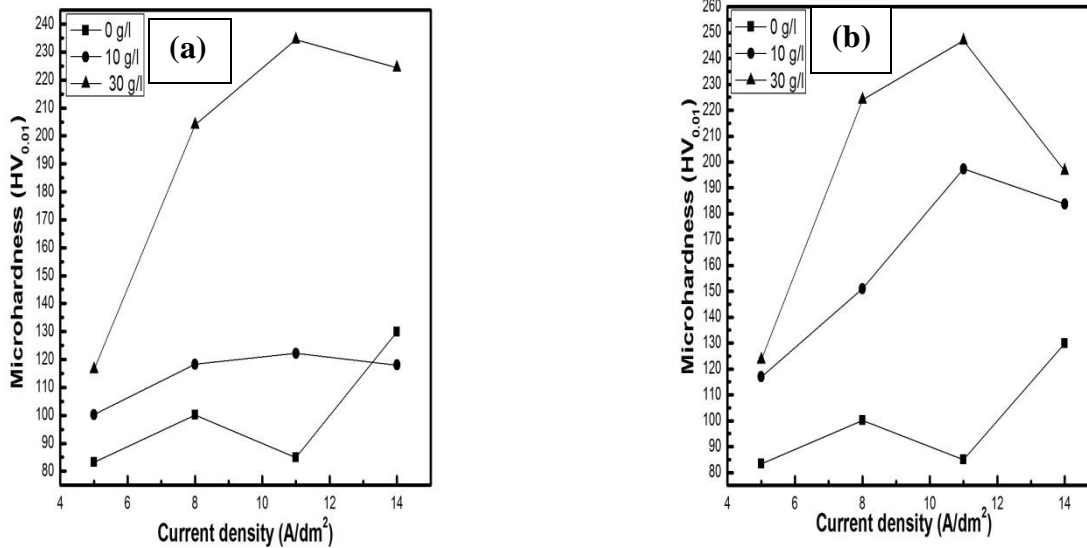
Figure 4.11: effect of current density on microhardness of (a) Cu-TiO$_2$ (b) Cu-Al$_2$O$_3$ coatings at current densities 5,8,11 and 14 A/dm^2.

In both the cases Cu-TiO$_2$ & Cu-Al$_2$O$_3$ the microhardness values obtained were followed the same trend. When the current density increased from 5 to 11 A/dm^2, the hardness values increased and at 14 A/dm^2 a little decrease in hardness values were obtained. In case of Cu-TiO$_2$ coatings at 5 A/dm^2 in both the cases 10 g/l, 30 g/l TiO$_2$ less hardness values were reported which is due to the random crystalline orientation (Table 4.1) which leads to decrease in the intensity of (220) texture, and increase in intensity of (200) plane this may be co related with [100] texture associated to deposits with minimum hardness and maximum ductility [73]. The minimum hardness for (200) diffraction line is attributed to lower angle between (200) and (100) planes, which leads to lower strain energy, the strain energy increases as the angle increases [74-75]. At 30 g/l and 5 A/dm^2 the hardness value obtained was less compare to 10 g/l titania, this is due to the increased intensity of (200) soft mode, increase in grain size and microstructure of the copper matrix, which looks as ropes like structure with loosely compacted. At 14 A/dm^2 also the same feature was observed as at 5 A/dm^2, the preferred (220) texture changes to (220)+(111) mixed preferred orientations, which leads to decrease in the intensity of (220) plane and increased intensity of soft mode (200) plane which is associated to [100] texture (soft mode) and also smaller amount of TiO$_2$ embedded in the composite coating which leads to decrease in

47

hardness values at this current density. The higher intensity of (220) plane leads to higher hardness this is due to its less active slip systems [76]. At 30 g/l TiO_2 as the current density increased from 8 to 11 A/dm^2 the wt% of TiO_2 increased from 0.78 to 1.51 which causes decrease in the intensity of (220) preferred direction from 96 to 75%, but improved hardness value due to the higher wt% TiO_2 (1.51wt%) embedded in the coating. At 8, 11 A/dm^2 current densities the increased wt% of TiO_2 modified the crystallite sizes from 56, 64 nm to 50, 41 nm which leads to the increased hardness values. In the present study at 11 A/dm^2 current density higher hardness values (122.2 HV at 10 g/l, 234.45 HV at 30 g/l) were obtained which is associated to preferred crystalline orientation and more amount of TiO_2 embedded in the composite coating and grain refinement.

In $Cu-Al_2O_3$ system the Hardness values obtained were higher compared to $Cu-TiO_2$ system this may be attributed to smaller amount of Copper oxide formation in the $Cu-Al_2O_3$ composite coatings which has higher hardness compare to copper. Current density and hardness relationship obtained in $Cu-Al_2O_3$ system is same as in $Cu-TiO_2$ system. At 8, 11 A/dm^2 the increased wt% Al_2O_3 in the coating changed the preferred (220) orientation to (220)+(311) mixed preferred orientations. Larger hardness values were obtained at 11 A/dm^2 in both 10 g/l (197.3HV) and 30 g/l (247HV) which is attributed to higher amount of Al_2O_3. In the present range of study at 30 g/l, 11 A/dm^2 shows highest hardness values in both $Cu-TiO_2$ and $Cu-Al_2O_3$ systems due to the higher incorporation of dispersed second phase particles and texture effect.

4.6.2 Wear study

The wear test on the surfaces of the composite coatings and coatings without addition of second phase particles were carried out by using DUCOM TR-208-M1 ball on plate wear tester by applying load 5 N for 5minutes with 10 rpm sliding speed on a 2 mm diameter track. The below Figure 4.12 (a) & (b) shows the comparable wear lose graphs (in terms of vertical penetration of the indenter or wear depth) as a function of sliding distance of Cu- 10 g/l TiO_2, Cu- 30 g/l TiO_2, and without TiO_2 at the current densities of 11 A/dm^2, 14 A/dm^2. The wear performance of electroplated composite films is known to be mainly dependent on the microstructure of the metal matrix as well as on the amount and distribution of incorporated particles [71, 72]. That is the wear behavior is co related to the hardness of the surface. According to the above statement the wear loss or extent should be high for pure copper (without oxide particles), and also for

lower wt% TiO_2 embedded samples. The below Figure 4.12 (a) & (b) shows exactly the same, wear loss of without TiO_2 samples is higher than composite coatings at 11, 14 A/dm^2 due to its low hardness and absence of dispersed hard ceramic oxide particles. At 10 g/l TiO_2 and 11, 14 A/dm^2 current densities the wear lose is high than samples at 30 g/l TiO_2 due to the lower wt% TiO_2 (Table 4.4) in the coatings and less hardness of the coating surfaces. The wear lose behavior of the coatings developed at current densities 5, 8 A/dm^2 followed the same trend as the microhardness showed. From the Figure 4.12 it can also observed that the wear lose of annealed copper (73.33 µm) is higher than the pure copper (68.5 µm) which can be attributed to the softness of annealed sample and also the loss is high (72.6 µm) for pure copper coating developed at 11 A/dm^2 than the coating developed at 14 A/dm^2 (47.6µm) which is due to the lower hardness of coating deposited at 11 A/dm^2 which has shown increased intensity of (200) line corresponds to (100) (soft mode).

(a)   (b)

Figure 4.12: Comparable wear plots between wear depth and sliding distance of Cu- 10 g/l TiO_2, Cu- 30 g/l TiO_2 and without TiO_2 coatings (a) at 11 A/dm^2 (b) at 14 A/dm^2 current densities.

Below Figure 4.13a & b shows plots of the comparable wear lose (in terms of vertical penetration of the indenter or wear depth) as a function of sliding distance of Cu- 10 g/l Al_2O_3, Cu- 30 g/l Al_2O_3, and without Al_2O_3 at the current densities of 11A/dm^2, 14A/dm^2. The below Figure shows the similar trend for Al_2O_3 incorporation as observed for TiO_2 incorporation.

In case of some graphs momentary negative slope could be observed. This may due to cold welding of soft Cu phase with the hardened steel ball (indenter) resulting in decrease in the wear depth. In general it be concluded that, with increase in ceramic powder contents, the wear resistance of Cu coating increases.

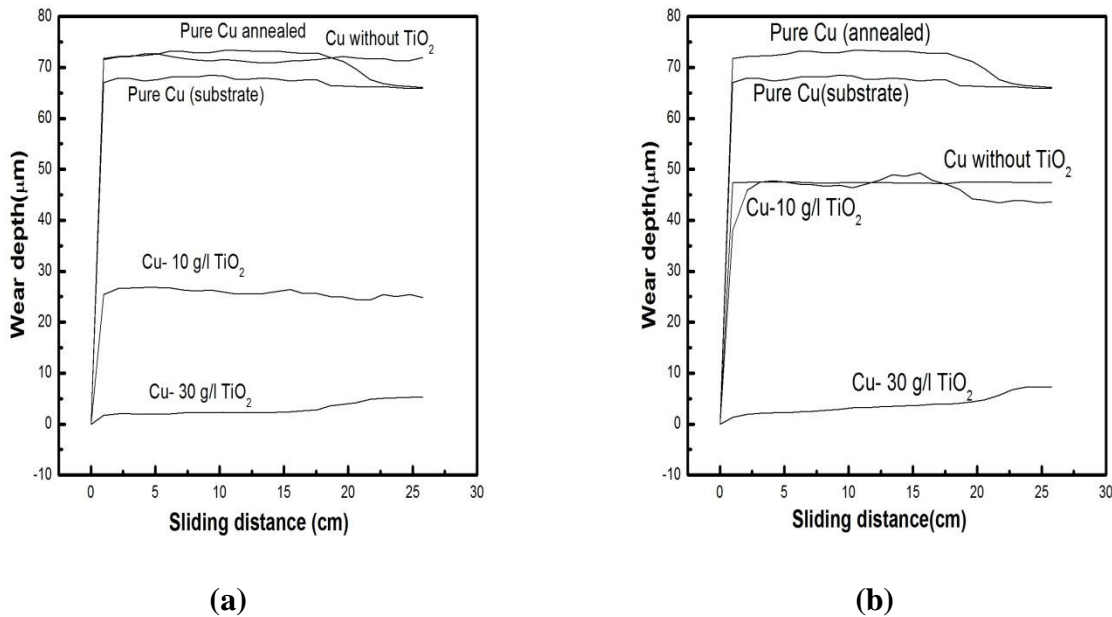<center>(a)   (b)</center>
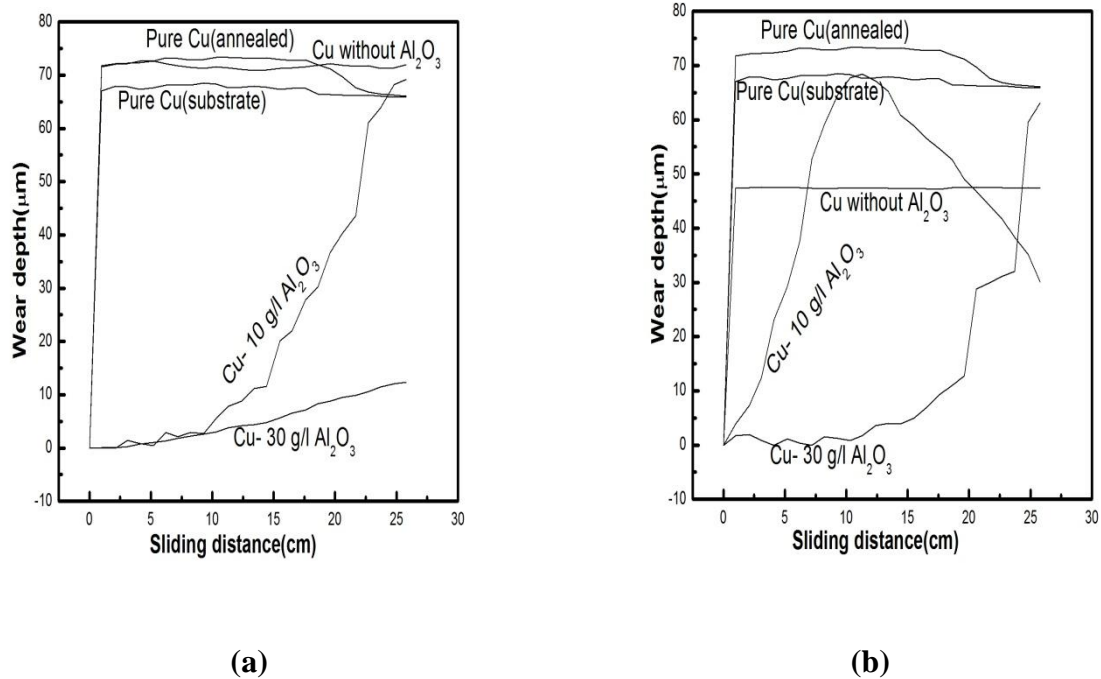
Figure 4.13: Comparable wear plots between wear depth and sliding distance of Cu- 10 g/l Al_2O_3, Cu- 30 g/l Al_2O_3 and Cu without Al_2O_3 coatings (a) at 11 A/dm^2 (b) 14 A/dm^2.

Figure 4.14 shows the SEM micrographs of the worn surfaces of wear tested samples. Figure (a), (b) & (c) shows the overall wear track of the worn wear surfaces where as Figure (d), (e) & (f) shows the same wear track at higher magnification of Cu substrate, pure Cu without oxide powder at 11 A/dm^2 and Cu-10 g/l TiO_2 at 11A/dm^2. From the figure it can be seen that in case of pure copper (substrate) the wear track width is huge and also the track is not smooth. This can be attributed to the inherent ductility and softness of the copper. Slight less wear track width was observed for copper coating without ceramic oxide at11 A/dm^2 current density. Whereas the track width is very small for Cu-TiO_2 coating developed at 11 A/dm^2 current density, this is due to the presence of dispersed second phase TiO_2 particles in the copper matrix which improves the hardness of the surface. Wear track with ceramic embedded surface shows more rubbing mark due to three body motion (abrasion by the worn out ceramic particles). So, it can be concluded

<center>50</center>

that addition of ceramic oxide marginally transforms the wear nature from adhesive to abrasive type.

Figure 4.14: SEM micrographs of wear track of (a) substrate (pure Cu) (b) Pure copper (without ceramic oxide) at 11A/dm^2 (c) Cu- 10 g/l TiO$_2$ at 11 A/dm^2 current density and (d), (e) & (f) SEM micrographs of same wear tracks at higher magnification.
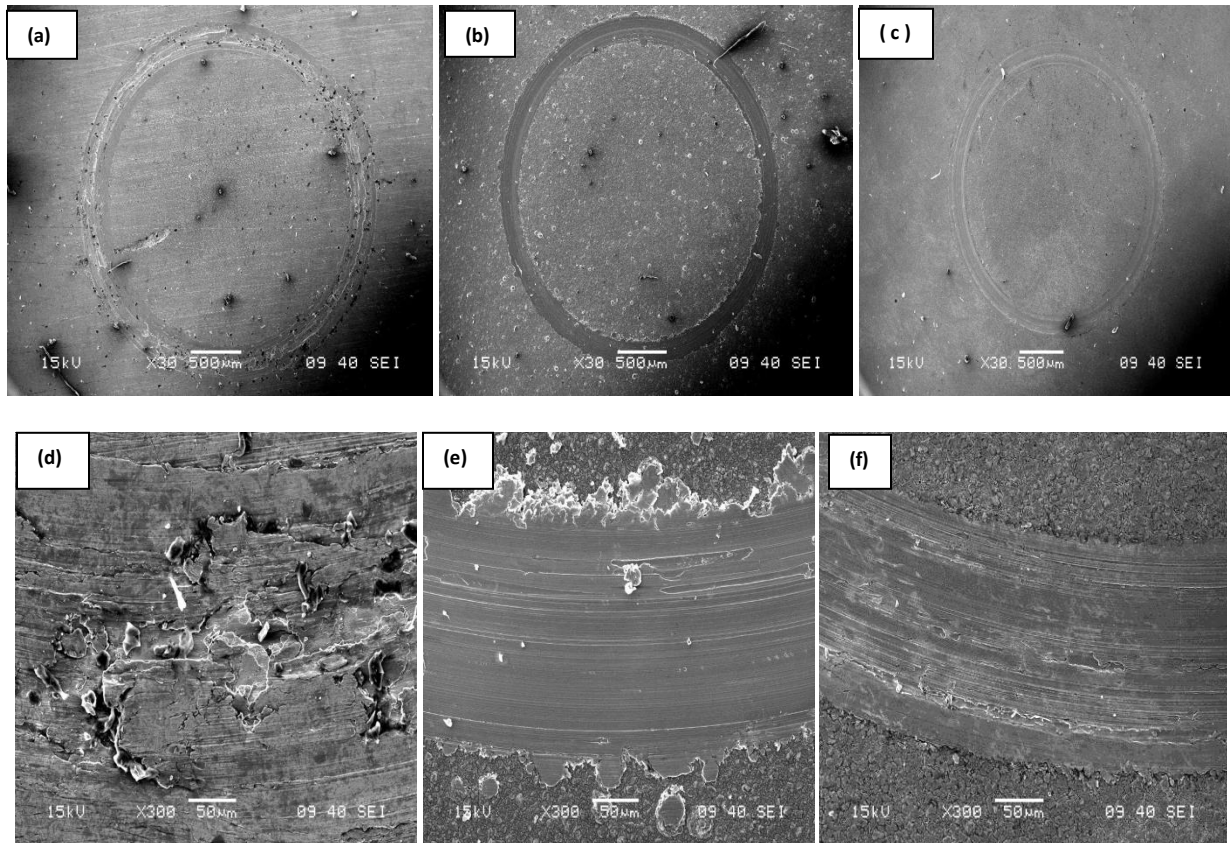
4.7 Brief comparison of TiO_2 and Al_2O_3 systems

Both the systems studied in the present study shows similar trend in general as discussed in the previous sections. But minute differences can be observed in various chracatezition results resulting in different final properties. Breif account of such variations are discussed below.

In case of Cu-TiO_2 system at 10 and 30 g/l powder concentration (220) plane is more pronounced, where as in case of Cu-Al_2O_3 system it is shifted to (220)+(311) mixed orientation. With 10 g/l Al_2O_3 in bath at all current densities smaller crystallite sizes were observed compared to 10 g/l TiO_2 in bath. Grain size refinement was observed in case of Cu-TiO_2 system at 30 g/l TiO_2 concentration and 11, 14 A/dm^2 current densities, whereas no such type of feature was obtained for Cu-Al_2O_3 system. In both the systems at 5 A/dm^2 random crystalline orientation was obtained with (220) having little higher intensity.

In case of Cu-TiO_2 system at 10 & 30 g/l TiO_2 in bath with 11 A/dm^2 current density moderate wt% TiO_2 (Ti=0.70 & 1.51 wt.%) was co deposited in the Cu-TiO_2 coatings, where as with same conditions for Cu-Al_2O_3 system Al_2O_3 amount was higher (Al=2.21 & 4.49 wt.%) in the coatings.

Higher hardness values were resulted in case of Cu-Al_2O_3 system compared Cu-TiO_2 system at both the concentrations. This may be due to lower co deposition of TiO_2 compared to Al_2O_3.

Similar effects were observed during wear testing of 10 g/l loaded samples, i.e. wear resistance in general is better for Al_2O_3 composite coating mainly at initial sliding distance. After certain amount of sliding TiO_2 shows better result.

Chapter 5

Conclusions

Conclusions

Scope of future work

CHAPTER 5

CONCLUSIONS

5.1 Conclusions

In the present study, $Cu-TiO_2$ and $Cu-Al_2O_3$ nanocomposite coatings were developed successfully by using Electrodeposition process on the Copper substrate from copper sulfate bath. From the detailed investigation of the results obtained, the following conclusions can be drawn:

1. The particle size and zeta potential of TiO_2 and Al_2O_3 were determined by using Zetasizer and the particle size obtained was ~202 nm and ~287 nm respectively. And the iso electric points were around 4.2 pH for TiO_2 and around 5.3 pH for Al_2O_3.

2. From the XRD patterns, Tetragonal and Rhombohedra crystal structures of TiO_2 and Al_2O_3 respectively were confirmed. The XRD peaks of both powders does not show appreciable peak broadening though the sizes of both particles are in nanometric size, as the powder were synthesized by a chemical route which does not introduced strain into the material. The XRD pattern of $Cu-TiO_2$ and $Cu-Al_2O_3$ coatings does not show TiO_2 and Al_2O_3 peaks clearly with much intensity because of less wt% (less than 10%) of powders embedded in the composite coatings. The $Cu-Al_2O_3$ XRD pattern also showing the peaks of Copper Oxide (Cu_2O, JCPDS Reference No: 05-0667) with very less intensity.

3. From the Texture calculations of Cu a strong (220) texture was obtained for composite coatings and pure copper depositions, the intensity of (220) texture and shift of this texture plane to mixed plane orientations was obtained due to the particle incorporation, the current density and Cu_2O in $Cu-Al_2O_3$. At 8, 11 A/dm^2 current density, 10 and 30 g/l Al_2O_3 in the bath along with (220) texture (311) preferred plane is also observed. Whereas a (111) texture was observed for substrate (pure copper). The crystallite size was calculated by using Scherrer formula from (111) peak and was below 100 nm for all the coated samples.

4. The Energy Dispersive Spectrum (EDS) of $Cu-TiO_2$ and $Cu-Al_2O_3$ coatings gives evidence of presence of Cu, O_2, Ti, Al. From the Scanning Electron Microscope (SEM) surface morphologies obtained the coating surfaces observed at all deposition parameters were

smooth, no dendrites, cracks and nodule like structures were observed on the surfaces. As no surfactant is added to the bath, agglomeration of the particles was observed in the copper matrix. In case of Cu-TiO$_2$ coatings at lower current densities (5, 8 A/dm^2) the coatings were fully compacted whereas at current densities 11, 14 A/dm^2 the surfaces has cauliflower like structures. In case of Cu-TiO$_2$ at current density 5 A/dm^2, 30 g/l TiO$_2$ in bath, different morphology, rope like structure with voids and un compacted feature was obtained. In case of Cu-Al$_2$O$_3$ at 30 g/l Al$_2$O$_3$ in bath, 5 A/dm^2 current density randomly oriented crystallites with loose packing was observed.

5. The microhardness values obtained for both the composite coatings are higher than the pure copper hardness, the improvement is attributed to dispersion strengthening caused by the embedded second phase particles, texture and modified microstructure of copper matrix. For Titania, there is maximum of 1.28 and 2.46 times increase, for Alumina there was maximum of 2.07 and 2.6 times increase in microhardness after addition of dispersion with respect to substrate and pure copper deposition respectively was observed. At moderate current densities (8, 11 A/dm^2) higher hardness values were observed.

6. The wear resistance of the composite coatings was higher than the substrate, annealed and un reinforced copper. The wear resistance improved with increased weight % of dispersed second phase particles in the bath compared to unreinforced copper coatings. The increase in wear resistance is due to the dispersed second phase particles and improved hardness which decreases friction between the steel ball and the coating surface. The addition of ceramic oxide particles marginally transforms the wear from adhesive (unreinforced copper) to abrasive type.

5.2 Scope of Future work

Due to the unstable data, results of Electrical resistivity measurement could not be reported. It is one of the important future works that can be carried out to justify the application of these coatings to electrical components.

Chapter 6

References

CHAPTER 6

REFERENCES

1. Smithells Metals Reference Book (7th edition), edited by E A Brandes and G B Brook, Butterworth-Heinemann, Oxford, 2000. Mechanical Metallurgy, by: G E Dieter, McGraw Hill, Singapore, 1988.

2. Lawrence J. Durney, Electroplating Engineering Handbook, 4th edition, Van Nostrand Reinhold Company, 1984, pp. 364.

3. Yuttanant Boonyongmaneerat, Kanokwan Saengkiettiyut, et[al]., Effects of WC addition on structure and hardness of electrodeposited Ni–W, Surface & Coatings Technology, 203, (2009) pp. 3590–3594.

4. Injeti Gurrappa and Leo Binder, Electrodeposition of nano structured coatings and their characterization—a review, Sci. Technol. Adv. Mater. 9, (2008), 043001 (11pp).

5. Low C.T.J., Wills R.G.A., Walsh F.C., Electrodeposition of composite coatings containing nanoparticles in a metal deposit, Surface & Coatings Technology 201, (2006), pp. 371–383.

6. Hong-Kee Lee, Ho-Young Lee, Jun-Mi Jeon, Codeposition of micro- and nano-sized SiC particles in the nickel matrix composite coatings obtained by electroplating, Surface & Coatings Technology, 201, (2007), pp. 4711–4717.

7. Gul. H, Kilic. F¸ Aslan. S, Alp. A, Akbulut. H, Characteristics of electro-co-deposited Ni–Al_2O_3 nano-particle reinforced metal matrix composite (MMC) coatings, Wear 267, (2009), pp. 976–990.

8. Stojak. J.L, Fransaer. J, Talbot. J. B, Review of Electrocodeposition, in: R.C. Alkire, D.M. Kolb (Eds.), Adv. Electrochem. Sci. Eng. Wiley-VCH Verlag, Weinheim, 2002.

9. Saha. R.K, Khan. T.I, Effect of applied current on the electrodeposited Ni–Al_2O_3 composite coatings, Surface & Coatings Technology, (2010).

10. Rashidi. A.M, Amadeh. A, The effect of current density on the grain size of electrodeposited nanocrystalline nickel coatings Surface & Coatings Technology, 202, (2008), pp. 3772–3776.

11. Stankovic. V.D, Gojo.M, Electrodeposited composite coatings of copper with inert, semiconductive and conductive particles, Surface and Coatings Technology, 81, (1996), pp. 225-232.

12. Mechanical Metallurgy, by: G E Dieter, McGraw Hill, Singapore, 1988.

13. Paul M. Unterweiser (ed.), in 'Source Book on Copper and Copper Alloys', ASM, Metals Park, Ohio, 1979, p. 5, 333.

14. E. G. West (ed.), in 'Copper and its Alloys', Ellis Horwood, Chichester, 1982, p.125.

15. Bauccio, Michael (Ed.). ASM Metals Reference Book, Third Edition. Materials Park, Ohio: ASM International, p. 445.

16. Chattopadhyay. R "Advanced Thermally Assisted Surface Engineering Processes" Kluwer Academic Publishers, MA, USA (now Springer, NY), 2004.

17. Kennedy D.M, Xue. Y, and Mihaylova. E, Current and Future Applications of Surface Engineering, The Engineers Journal (Technical), vol. 59, (2005), pp 287-292.

18. Brenner, A. and Riddell. G, Deposition from Aqueous solution: An overview, J. Res. Natl. Bureau of Standards, 39, November 1947.

19. Hitchman M.L, Jensen K.F, Chemical Vapor Deposition—Principles and Applications, Academic Press, London, 1993.

20. Sherman. A, Chemical Vapor Deposition For Microelectronics—Principles, Technology and Applications, Noyes Publications, New Jersey, 1987.

21. Viswanathan. V, Laha. T, Balani. K, Agarwal. A, Seal. S, Challenges and advances in nanocomposite processing techniques Materials Science and Engineering R 54, (2006), pp. 121–285.

22. Nanostructured materials processing, properties and applications, by C.C.Koch, Noyes publications, Chapter 5- Electrodeposited Nanocrystalline materials, 2002, pp. 179-222.

23. Gleiter, H., in: Deformation of Polycrystals: Mechanisms andMicrostructures, Proc. 2nd Riso Int. Symp. on Metallurgy and Materials Science, p. 15, Riso National Laboratory, Roskilde, Denmark (1991).

24. Clark. D, Wood. D and Erb. U, Industrial applications of electrodeposited nanocrystals, NanoStruetured Materials. Vol. 9, 1997, pp. 755-758.

25. Schuh. C.A, Nieh. T.G, Iwasaki. H, The effect of solid solution W additions on the mechanical properties of nanocrystalline Ni, Acta Materialia, 51, (2003), pp. 431–443.

26. Cziraki. A, Fogarassy. B, Gerocs. I, Toth-Kadar. E, and Bakonyi. I, microstruclure and growth of electrodeposited nanocrystalline nickel foils, J. Mater. Sci., 29, 994, pp. 4771-4777.

27. Bockris. J.O.M, and Razumney. G.A, Fundamental Aspects of Electrocrystallization, p.27, Plenum Press, New York (1967).

28. Chow. G.M, *et al.*, (eds.), Nanostructured Films and Coatings, Kluwer Academic Publishers. Printed in the Netherlands, 2000, pp.11-24.

29. Luisa Peraldo Bicelli, Benedetto Bozzini, Claudio Mele, Lucia D'Urzo, A Review of Nanostructural Aspects of Metal Electrodeposition, Int. J. Electrochem. Sci., 3, (2008), pp. 356 – 408.

30. Erb. U, Electrodelqslted nanocrystals: syntresis, properties and indusiiual applications, NanoStruchued Matiab, Vol. 6, 1995, pp. 533-538.

31. Hanzhuo Zhang, Zhonghao Jiang, Yinghuai Qiang, Microstructure and tensile deformation of nanocrystalline Cu produced by pulse electrodeposition, Materials Science and Engineering A 517, (2009), pp. 316–320.

32. Shanthi. C, Barathan. S, Rajasrisen Jaiswal, Arunachalam. R.M, Mohan. S, The effect of pulse parameters in electro deposition of silver alloy, Materials Letters, 62, (2008), pp. 4519–4521.

33. Xi Zhang, K. N. Tu, Zhong Chen, Y. K. Tan, C. C. Wong,et al., Pulse Electroplating of Copper Film, A Study of Process and Microstructure, Journal of Nanoscience and Nanotechnology, Vol.8, 2008, pp. 2568–2574.

34. Wonbaek kim and Rolf well, Pulse plating effects in nickel electrodeposition, Surface and Coatings Technology, 38, (1989), pp. 289 – 298.

35. Gyana R. Pattanaik, Dinesh K. Pandya and Subhash C. Kashyap, Preparation of Cu-Co Alloy Thin Films on n-Si by Galvanostatic DC Electrodeposition, J. Electrochem. Soc., Volume 149, Issue 7, 2002, pp. C363-C369.

36. Laxmidhar Besra, Meilin Liu, A review on fundamentals and applications of electrophoretic deposition (EPD), Progress in Materials Science 52, (2007), pp. 1–61.

37. Hasegawa K, Kunugi S, Tatsumisago M, Minami T. Preparation of thick films by electrophoretic deposition using modified silica particles derived by sol–gel method, J Sol–gel Sci Technol, 1999, 15:243–9.

38. Shan W, Zhang Y, Yang W, Ke C, Gao Z, Ke Y, et al. Electrophoretic deposition of nano-size zeolites in non-aqueous medium and its application in fabricating thin zeolite membranes. Micropor Mesopor Mater, 69, 2004, pp. 35–42.

39. Wei M, Ruys AJ, Milthorpe BK, Sorrell CC, Evans JH. Electrophoretic deposition of hydroxyapatite coatings on metal substrate: a nano-particulate dual coating approach, J Sol–gel Sci Technol, 21, 2001, pp.39–48.

40. Sridhar TM, Mudali UK. Development of bioactive hydroxyapatite coatings on Type 316L stainless steel by electrophoretic deposition for orthopaedic applications, Trans Ind Inst Met , 2003, 56(3), 221–30.

41. Shane MJ, Talbot JB, Kinney BG, Sluzky E, Hesse HR. Electrophoretic deposition of phosphors: II deposition experiments and analysis, J Colloid Interface Sci, 1994, 165,334–40.

42. Shane MJ, Talbot JB, Schreiber RG, Ross CL, Sluzky E, Hesse KR. Electrophoretic deposition of phosphors: I conductivity and zeta potential measurements, J Colloid Interface Sci ,1994, 165, 325–33.

43. Jean L. Stojak, Jan Fransaer and Jan B. Talbot, Review of Electrocodeposition, Advances in Electrochemical Science and Engineering, Volume 7, Edited by Richard C. Alkire, and Dieter M. Kolb, 2001 Wiley-VCH Verlag GmbH.

44. Ebdon. P.R, The Performance of Electroless Nickel–PTFE Composites, Plating and Surface Finishing, 75 (9), (1988), pp. 65–68.

45. Xinying Lu, Rizhang Zhu and Yedong He, Electrophoretic deposition of MCrAlY overlay-type coatings, Oxidation of metals, vol 43, Nos 3/4, 1995.

46. Jean. L, Stojak and Jan B. Talbot, Effect of particles on Polarization during Electrocodeposition using a Rotating Cylinder Electrode, Journal of Applied Electrochemistry, Volume 31, Number 5, pp. 559-564.

47. Metzger. W, Ott. R, Laux. G, *et al.*, Electrodeposition of dispersion hardened nickel, Galvanoteknik (in German), 61, (1970), No.12, p.998.

48. Catalina Iticescu, Geta Carac, Olga Mitoseriu and Thomas Lampkt, Electrochemical deposition of composite coatings in copper matrix with TiO_2 nanoparticles, Revue Roumaine de Chimie, 53(1), 2008, pp. 43–47.

49. Nowak. P, Socha. R.P, Kaisheva. M, Fransaer. J, Celis. J.P, and Stoinov. Z, Electrochemical investigation of the codeposition of SiC and SiO_2 particles with nickel, Journal of Applied Electrochemistry, Volume 30, Number 4, pp. 429-437.

50. Saha. R.K, Khan. T.I, Effect of applied current on the electrodeposited $Ni–Al_2O_3$ composite coatings, Surface and coating technology, 205, 2010, pp. 890-895.

51. Low. C.T.G, Wills. R.G.A, Walsh. F.C, Electrodeposition of composite coatings containing nanoparticles in a metal deposit, Surface & Coatings Technology, 201, (2006), pp. 371–383.

52. Jianhua Zhu, Lei Liu , Guohua Hu , Bin Shen , Wenbin Hu and Wenjiang Ding, Study on composite electroforming of Cu/SiCp composites, Materials Letters, 58, 2004, pp. 1634-1637.

53. Lozano-Morales. A and Podlaha. E.J, The Effect of Al_2O_3 powder on Cu Electrodeposition, J.Electrochem. Soc., Volume 151, 2004, Issue 7, pp. 478- 483.

54. Medelien. V, The influence of B_4C and SiC additions on the morphological, physical, chemical and corrosion properties of Ni coatings, Surface and Coatings Technology, Volume 154, Issue 1, 1 May 2002, pp. 104-111.

55. Steven J. Osborne, Wendi S. Sweet, Kenneth S. Vecchio, and Jan B. Talbot, Electroplating of Copper–Alumina Nanocomposite Films with an Impinging Jet Electrode, J. Electrochem. Soc., Volume 154, 2007, Issue 8, pp. D394-D399.

56. Ramalingam. S, Muralidharan. V.S & Subramania. A, Electrodeposition and characterization of Cu-TiO$_2$ nanocomposite coatings, J Solid State Electrochem, (2009), 13, pp. 1777–1783,

57. Andreas Bund and Denny Thiemig, Influence of bath composition and pH on the electrocodeposition of alumina nanoparticles and copper, Journal of Applied Electrochemistry (2007), 37, pp. 345–351.

58. I. Zamblau *et al*., Corrosion Behavior of Composite Coatings obtained by electrolytic codeposition of Copper with Alumina nanoparticles, Chem. Biochem. Eng., Q. 23 (1), 2009, pp. 43–52,

59. Roos. J.R, Celis. J.P and H. Kelchtermans, Dispersion-hardened electrolytic Copper-alumina coatings, Thin Solid Films, 54, (1978), pp. 173-182.

60. Benjamin D. Craig, Material failure modes, part II: A brief tutorial on impact, spalling, wear, brinelling, thermal shock, and radiation damage, Journal of Failure Analysis and Prevention , Volume 5, Number 6, 7-12, DOI: 10.1361/154770205X76240.

61. Stachowiak, G. W., and A. W. Batchelor (2005). Engineering Tribology. Burlington, Elsevier Butterworth-Heinemann.

62. Mamata, K. P. (2008). "A review on silt erosion in hydro turbines." Renewable & sustainable energy reviews, 12(7), 1974.

63. Sho Kataoka, Marc C. Gurau, Fernando Albertorio, et al., Investigation of Water Structure at the TiO$_2$/Aqueous Interface, Langmuir , 20, 2004, pp. 1662-1666.

64. Bimal P. Singh, Ruben Menchavez, Chika Takai, Masayoshi Fuji, Minoru Takahashi, Stability of dispersions of colloidal alumina particles in aqueous suspensions, Journal of Colloid and Interface Science 291, (2005), pp. 181–186.

65. Klug.H.P, Alexander. L.E, X-Ray Diffraction Procedures, Chapman and Hall, London, 1954, Chapter 9.

66. Abdel Aal. A, Hassan. H.B, Electrodeposited nanocomposite coatings for fuel cell application, Journal of Alloys and Compounds, 477, (2009), pp. 652–656.

67. Lajevardi. S.A, Shahrabi. T, Effects of pulse electrodeposition parameters on the properties of Ni–TiO$_2$ nanocomposite coatings, Applied Surface Science, 256, (2010), pp. 6775–6781.

68. Denny Thiemig, Andreas Bund, Characterization of electrodeposited Ni–TiO$_2$ nanocomposite coatings, Surface & Coatings Technology 202, (2008), pp. 2976–2984.

69. Lajevardi. S.A and Shahrabi. T, Effects of pulse electrodeposition parameters on the properties of Ni–TiO$_2$ nanocomposite coatings, Applied Surface Science, Volume 256, Issue 22, 1 September 2010, pp. 6775-6781.

70. Denny Thiemig, Ronny Lange, Andreas Bund, Influence of pulse plating parameters on the electrocodeposition of matrix metal nanocomposites, Electrochimica Acta, 52, (2007), pp. 7362–7371.

71. Hou. K.H, Ger. M.D, Wang. L.M, Ke. S.T, The wear behaviour of electro-codeposited Ni–SiC composites, Wear 253, (2002), pp. 994–1003.

72. Aruna. S.T, William Grips. V.K, Rajam. K.S, Ni-based electrodeposited composite coating exhibiting improved microhardness, corrosion and wear resistance properties, Journal of Alloys and Compounds 468, (2009), pp. 546–552.

73. DhananjayKumar Singh and V. B. Singh, Electrodeposition of Ni–SiC Composite from a Non-Aqueous Bath, J. Electrochem. Soc., Volume 158, 2011, pp. D114-D118.

74. Jian-Min Zhang *et al*. General compliance transformation relation and applications, for anisotropic cubic metals,   Materials Letters, 62, (2008), pp. 1328–1332.

75. Jian Feng Wang *et al*. Evolution of Residual Stress in Cu-Line Patterns with Different Linewidth, Advanced Materials Research, 609, 2010, pp. 89-91.

76. Vipin chawla, jayaganthan R and Ramesh Chandra, Microstructural characteristics and mechanical properties of magnetron sputtered nanocrystalline TiN films on glass substrate Bull. Mater. Sci., Vol. 32, No. 2, April 2009, pp. 117–123.